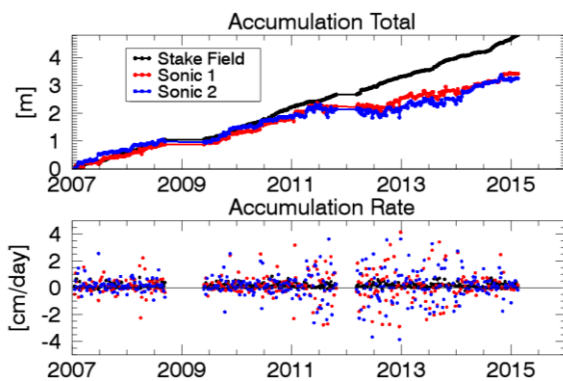


ESA Contract
4000121829/17/NL/FF/mg

Technical Support for the SnowSum Experiment

Final Report



Snowfall accumulation at Summit Station (Greenland) from stake field and sonic observations. See section 3.1.1 for details.

Version: 1.01
Date: 2018/10/09

Technical Support for the SnowSum Experiment		INFERMUS	
Final Report	ESA Contract 4000121829/17/NL/FF/mg		

Title image caption	Snowfall accumulation at Summit Station (Greenland) from stake field and sonic observations. See section 3.1.1 for details.		
Project	Technical Support for the SnowSum Experiment ESA Contract No. 4000121829/17/NL/FF/mg		
Client	European Space Agency (ESA), ESTEC Keplerlaan 1 NL-2201 AZ Noordwijk http://www.esa.int		
Main contractor	Informus GmbH Brehmestr. 50 D-13187 Berlin http://www.informus.de		
Title of document	Final Report		
Author(s) of document	Ralf Bennartz, Frank Fell		
Status	Released		
Distribution	INF, ESA		
Version control	2018/02/26	0.50	Intermediate report presenting results from Tasks 1 and 2.
	2018/06/06	0.90	Draft final report, additionally including results from Tasks 3 and 4
	2018/10/09	1.00	Final version, fully revised
	2018/10/09	1.01	ESA contract number added to header and title page

Table of contents

1	Introduction.....	8
1.1	Acronyms	8
1.2	Background	8
1.3	Aims and objectives	9
1.4	Structure of the document.....	9
2	Observational data used in this study	10
2.1	ICECAPS	11
2.2	PROMICE	11
2.3	GC-NET observations	12
2.4	CloudSat observations	13
3	Temporal and spatial variability of snowfall over the GrIS	15
3.1	Temporal variability of precipitation at Summit from ICECAPS	15
3.1.1	Snowfall accumulation from sonic and stake field.....	15
3.1.2	Precipitation type	16
3.1.3	Consistency between MMCR and POSS radar observations	18
3.1.4	Radar-derived precipitation – impact of Z-S relation	19
3.2	Evaluation of the use of space-borne radar for precipitation studies	22
3.2.1	Effects and removal of ground clutter	22
3.2.2	Impact of height of observations above ground on estimated surface snowfall rate.....	26
3.2.3	Impact of Z-S relation.....	28
3.2.4	Comparison against stake field	29
3.2.5	Final form of CloudSat snowfall retrieval over the GrIS	31
3.2.6	Comparison against GC-NET and PROMICE	32
3.3	Spatial and seasonal variability of snowfall over the GrIS	33
3.4	Snowfall by drainage system.....	38
3.5	Annual cycle of snowfall at Summit.....	40
3.6	Relation between liquid equivalent snowfall rate and snow water equivalent (SWE).....	41
4	Science potential of observations in support of future missions	43
5	References.....	45
	Appendix A: GC-NET and PROMICE datasets and data formats.....	47
	Appendix B: ICECAPS datasets and data formats	48
	Appendix C: CloudSat monthly mean liquid equivalent snowfall rates	49

List of figures

- Figure 1: Location of all surface stations used in this study. GC-NET stations are depicted in red, PROMICE stations in blue, and ICECAPS (coincident with the GC-NET ‘Summit’ station) is shown as the larger orange circle near the centre of Greenland. The station list on the right is latitude-ordered. 10
- Figure 2: Example observations from PROMICE station NUK_L, corresponding to the red dot in the upper left image. The blue dots in the upper left plot indicate the locations of all other PROMICE stations. The upper right plot shows the observed monthly and hourly averaged shortwave (SW) downward flux at the surface, the lower left plot shows the surface skin temperature derived from observed upwelling infrared surface observations, and the lower right plot shows the SW atmospheric transmission estimated from the SW downward flux at the surface and the incoming solar radiation at the top of the atmosphere. In the lower left plot, yellow to red colours indicate surface skin temperatures above freezing, while white reflects temperatures below -10 °C. 12
- Figure 3: Number of CloudSat observations per month all over Greenland (top) and within 50 km of Summit Station (bottom). 13
- Figure 4: CloudSat data density over Greenland at 1 × 2 degrees (left, approximately 100 km × 100 km) and 0.025 × 0.045 degrees (right, approximately 2.5 km × 2.5 km). Shown is the total number of observations per grid box over the period from 2006 to 2016. 14
- Figure 5: GC-NET sonic derived and stake field derived total accumulation and accumulation rates at Summit Station. There are two sonics operating at each GC-NET station. 15
- Figure 6: Lidar and radar observations of a high-latitude precipitating weather system on July 13, 2015. The CALIOP lidar observations (with background blue) represent a satellite transect over Greenland. The radar observations are from the ICECAPS MMCR. One can distinguish two different types of precipitation. Precipitation associated with the low clouds (see location of blue arrows) is dominated by riming and diffusional growth of ice particles in a super-saturated environment. Precipitation in the deeper clouds forms largely by pure ice growth processes with little liquid water present (liquid water path known from ground-based collocated upward looking microwave radiometer observations). 16
- Figure 7: Multi-Angle Snowflake Camera (MASC) ICECAPS-observed surface snowfall size distribution compared to various size distributions typically used in modelling. The data were collected at Summit between June and August 2015. The blue curve shows an observed snowfall size distribution. The red curve is a fit to the size distribution using a combination of exponential relationships (Marshall-Palmer-like). Very small ice particles are not detected by the MASC. The insets show examples observed snowflakes at different stages of riming and aggregation. 17
- Figure 8: POSS-derived snowfall rates versus MMCR-derived radar reflectivities. The red line corresponds to the Z-S relation shown in Equation (1). The green line corresponds to the Z-S relation used in *Castellani et al.* [2015]. Each dot corresponds to a daily mean snowfall rate. 18

Figure 9: Comparison between snowpack accumulation rates from stake field and MMCR-derived or POSS-derived liquid equivalent accumulation rates. ‘EFF DENS’ is the effective density in $[kg/m^3]$ of the snowpack needed to explain the mean stake accumulation by the liquid equivalent precipitation from either MMCR or POSS. The lines start at $[0,0]$ and have the reported effective density (divided by 1000) as slope. Each data point corresponds to one week of observations as the snow stake heights are read of typically once a week. 20

Figure 10: The upper panel shows the POSS and MMCR-derived monthly mean liquid equivalent snowfall accumulation at Summit for the years 2010-2015. For MMCR the Z-S relation KB09_LR3 was used. The associated error bars give the minimum and maximum monthly mean values found over that same period. The lower plot shows how many years contributed to the upper plot for each month. 21

Figure 11: The left panel shows the mean elevation reported from CloudSat binned to 1×2 degrees. The right panel shows the elevation difference between IceBridge BedMachine v3 [Morlighem et al., 2017] and CloudSat. Note, that open water and sea ice observations are excluded from the dataset, so that differences observed near the coast only stem from ice-free land or GrIS observations within each grid box. 23

Figure 12: Histogram of occurrence of snowfall rate versus radar reflectivity for the entire CloudSat dataset over Greenland. The left panel shows the relation if the SNOWPROF surface snowfall rate is used face value. The right panel shows the relation with corrected topography. Different Z-S relations are shown as well. 24

Figure 13: The left panel shows the height of the CloudSat SNOWPROF ‘surface snowrate’ observation above the local topography (from IceBridge BedMachine). The right panel shows the difference between the height used in the revised product and original height. For example, at the southern tip of Greenland, the ‘surface snowrate’ reported in the SNOWPROF product comes from an actual altitude of about 1000 m above the surface. In the revised formulation discussed in the text, this height is pushed up by 500 m to 1500 m. 25

Figure 14: Impact of surface topography issues on cumulative snowfall rates. 25

Figure 15: The two left panels show histograms of MMCR observations at Summit. The left panel compares radar reflectivity at 135 m above the surface with the average radar reflectivity between 1000 and 1500 m above the surface, which corresponds to the height range where CloudSat observations are obtained. The middle panel shows a similar plot but with a height correction applied. See text for details. The right panel shows cumulative mean snowfall rates for the different radar reflectivities show in the left and middle plot. 26

Figure 16: Same as Figure 15 but for the DOE-ARM site at the North Slope of Alaska (NSA) at Barrow, Alaska. The figures are based on 1.08 million radar profiles obtained between 01/2008 and 4/2011. Only data for the winter months November through April are shown. The Barrow MMCR data were obtained from <https://www.archive.arm.gov/discovery/>. 27

Figure 17: Radar reflectivity at Ka-band (MMCR) and W-band (CloudSat) as function of snowfall rate for KB09_LR3 Z-S relation. The blue dashed curve has the same slope as the red curve and is shown only as a visual reference to see the slight difference in slope between the red and black curves..... 28

Figure 18: Cumulative snowfall rates derived from all CloudSat observations over Greenland. The thick black line corresponds to the CloudSat-derived surface snowfall rate from SNOWPROF with ground-clutter removed ('revised', same as in Figure 14). The other lines correspond to the Z-S relations applied to CloudSat reflectivities without height correction (left panel), and with height correction (right panel)..... 29

Figure 19: Same as Figure 9, but for CloudSat versus stake field..... 30

Figure 20: Total snowfall from CloudSat and stake field for all 369 weeks where data was available for both observation types. 31

Figure 21: Effective density of snowfall to explain surface accumulation from GC-NET or PROMICE by CloudSat snowfall. The table shows station name as well as elevation, and N: Number of months with valid data, C: Correlation between surface accumulation and CloudSat, D: effective density. The effective density at each site is also indicated on the map by its colour. 32

Figure 22: Density as function of mean station temperature for the 28 cases shown in Figure 21. The red and blue curves show results from *Fausto et al.* [2018] and *Reeh et al.* [2005]. 33

Figure 23: Annual mean liquid equivalent snowfall from CloudSat (left panel), ERA-Interim (2006-2016, middle panel), and the relative difference between both (right panel). 34

Figure 24: Annual cycle of liquid equivalent snowfall over the GrIS from CloudSat and ERA-Interim (top left panel), spatial correlation between the two (top right), mean bias (bottom left) and mean relative bias (bottom left). The dashed horizontal lines represent the annual average. 34

Figure 25: CloudSat-derived monthly mean snowfall rates..... 36

Figure 26: Same as Figure 25 but for ERA-Interim..... 37

Figure 27: Annual snowfall associated with the different drainage systems defined by *Zwally et al.*, [2012]. The upper left plot shows the mean annual snowfall, the upper right plot shows the fractional contribution to the total snowfall over the GrIS, the lower left plot shows the month of maximum precipitation as well as the drainage-basin identifier used in *Zwally et al.* [2012], and the lower right plot shows the amplitude of the annual cycle of snowfall. The month of maximum precipitation and amplitude are derived using a cosine fit to the annual cycle (see Figure 28)..... 38

Figure 28: Annual cycle of precipitation for the different drainage systems shown in Figure 27 for both CloudSat and ERA-Interim (2006-2016). The shaded area gives the uncertainty due to Z-S relation. The dashed curves give a cosine fit to the annual cycle. The numbers in brackets in the total are the fractional contribution of each drainage area to the total snowfall over the GrIS. Note the different scales of the y-axes. 39

Figure 29: Liquid equivalent snowfall over Summit from different data sources used in this publication. The shaded uncertainty range around the CloudSat estimates gives the uncertainty due to Z-S relation. The shaded uncertainty range around the stake field estimates gives the uncertainty due to different assumptions about snow density. The stake field estimates presented herein have been corrected for sublimation/deposition using ERA-Interim sublimation/deposition estimates. 40

Figure 30: Average number of months per year in which the maximum surface temperature never exceeded zero degrees Celsius in the period 2006-2016 based on ERA-Interim diurnal maximum temperatures. 42

List of tables

Table 1: Overview on datasets used in this study. The start and end dates refer to the actual start and end dates used in this study. Data collection for all ground-based datasets is ongoing.....	10
Table 2: Parameters of Ka-band (MMCR) and W-band (CloudSat) Z-S relations used in this study. The POSS operates at X-band so that the Z-S relation is not directly comparable the Z-S relations for MMCR.....	19
Table 3: Variables contained in surface_stations.nc.	47
Table 4: Variables contained in icecaps_data.nc.....	48
Table 5: Variables contained in cloudsat_1x2_degree.nc.....	49
Table 6: Variables contained in cloudsat_catchment.nc.....	49

1 Introduction

1.1 Acronyms

Acronym	Definition
AERI	Atmospheric Emitted Radiance interferometer
CALIOP	Cloud-Aerosol Lidar with Orthogonal Polarization
CAPABL	Cloud aerosol polarization and backscatter lidar
CPR	Cloud Profiling Radar
ECMWF	European Centre for Medium-Range Weather Forecasts
ESA	European Space Agency
GBI	Greenland Blocking Index
GC-NET	Greenland Climate Network
GrIS	Greenland Ice Sheet
HATPRO	Humidity and temperature profiler
ICECAPS	Integrated Characterization of Energy, Clouds, Atmospheric state, and Precipitation at Summit
LWP	Liquid water path
MASC	Multi-Angle Snowflake Camera
MMCR	Millimeter-wave Cloud Radar
NAO	North Atlantic Oscillation
netCDF	Network Common Data Format
NSF	National Science Foundation (US)
PIP	Processing implementation plan
POSS	Precipitation Occurrence Sensing System
PROMICE	Program for Monitoring of the Greenland Ice Sheet
SoW	Statement of Work
SW	Short wave
SWE	Snow Water Equivalent

1.2 Background

The SnowSum experiment is designed to support the development of future concepts to monitor the cryosphere by investigating and documenting the science potential of atmospheric precipitation time series together with other relevant long-term atmospheric observations over the Greenland Ice Sheet (GrIS).

Such atmospheric observations complement existing surface observations of snow accumulation or mass balance based on gravimetric or altimetry techniques, thereby providing an independent method of assessing snowfall.

1.3 Aims and objectives

This report identifies and describes the observational input data used in this study and provides feedback to the European Space Agency (ESA) on:

- Temporal and spatial variability of precipitation over the GrIS.
- The potential of utilizing space-borne precipitation together with ground-based measurements to obtain spatial and temporal distribution of snow depth.
- Evaluation and identification of gaps in the current coverage with a view on future cryosphere missions.

To achieve these objectives, the Statement of Work (SoW) to this study identifies four different tasks, namely:

- Task 1: Temporal variability of precipitation.
- Task 2: Spatial variability of precipitation over the GrIS using PROMICE (Program for Monitoring of the Greenland Ice Sheet) and GC-NET (Greenland Climate Network) data.
- Task 3: Initial evaluation of the use of space-borne precipitation radar observations for precipitation studies.
- Task 4: Initial evaluation of snow depth by means of precipitation accumulation from space-borne precipitation radar.

1.4 Structure of the document

The layout of this report reflects the studies' objectives: In section 2, the different input datasets are described in terms of instrumentation as well as temporal and spatial coverage. Section 3 provides the main data analysis and follows in its structure the four different tasks laid out in the SoW. Section 4 provides a gap analysis as well as an assessment of the datasets investigated in light of upcoming and planned satellite missions.

All data used for this study are provided in netCDF format. A detailed description of the datasets provided can be found in Appendices A, B, and C.

2 Observational data used in this study

This section describes the input datasets used in this study. We note that the datasets come from different sources and cover different time spans (Table 1).

Table 1: Overview on datasets used in this study. The start and end dates refer to the actual start and end dates used in this study. Data collection for all ground-based datasets is ongoing.

Dataset	Start date	End date	Comments
ICECAPS	07/2010	12/2015	Ongoing data collection as of January 2018
GC-NET	1995 (depends on station)	12/2015	Ongoing data collection as of January 2018
PROMICE	2007 (depends on station)	12/2015	Ongoing data collection as of January 2018
CloudSat	2006	2010 (2018)	Since 2010 with reduced functionality, near end of lifetime

The location and elevation of the different stations are shown in Figure 1. The three different station types (PROMICE, GC-NET, and ICECAPS) are discussed in detail below.

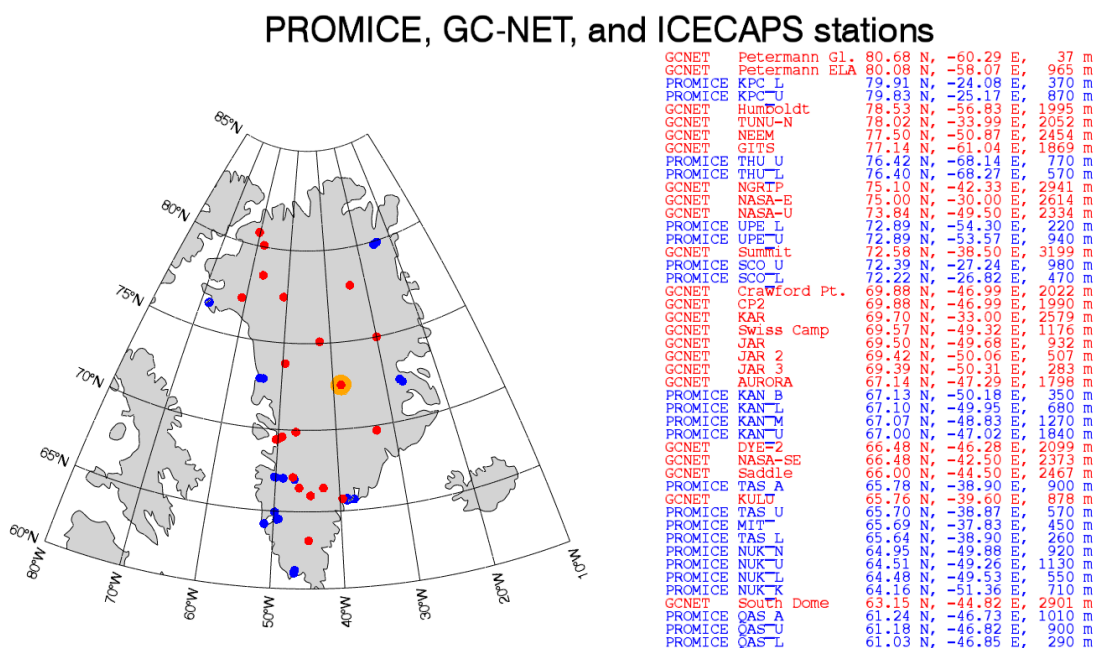


Figure 1: Location of all surface stations used in this study. GC-NET stations are depicted in red, PROMICE stations in blue, and ICECAPS (coincident with the GC-NET 'Summit' station) is shown as the larger orange circle near the centre of Greenland. The station list on the right is latitude-ordered.

2.1 ICECAPS

Since 2010, ICECAPS (Integrated Characterization of Energy, Clouds, Atmospheric state, and Precipitation at Summit, see <http://icecaps.ssec.wisc.edu/>) operates a sophisticated suite of instruments that observe properties of the atmosphere, clouds, and precipitation at Summit Station, located near the apex of the GrIS at an elevation of ca. 3,200 meters above sea level. These instruments have been operated from NSF's Mobile Science Facility, providing more than seven years of data as of spring 2017. This comprehensive dataset of atmospheric properties above the GrIS is unprecedented due to both the large number of distinct and complementary measurements that are being made and the completeness of the dataset.

The ICECAPS experiment as well as instrument specifications, measurements, and derived products are described in *Shupe et al.* [2013]. With respect to precipitation, of particular relevance are the Millimeter Cloud Radar (MMCR), the Precipitation Occurrence Sensor System (POSS), and the Multi-Angle Snowflake Camera (MASC, 2015 – 2016, selected dates only). In this study we build on earlier work by *Castellani et al.* [2015], and *Petterson et al.* [2017]. The latter study also provides a combined dataset of relevant parameters for studying precipitation variability over the central GrIS. This dataset is available with a temporal resolution of one minute and is used as a basis for the investigations performed here but complemented by additional MMCR observations.

In addition to these ICECAPS observations, other observations are available at Summit as well. Most important in the current context is the so-called 'stake field' consisting of 11×11 bamboo stakes that are planted in the snow a few hundred meters away from the station. The height of all 121 stakes above the snow surface is read off about every week, thereby creating a unique reference for surface height changes. Once a year, the stakes are raised by about 70 cm to allow for continuous measurements. These stake measurements go back to 2003, cover the full ICECAPS period and provide a rare independent set of observations of snowfall accumulation. Similar to *Castellani et al.* [2015], who also provide a discussion on the accuracy of the stake field data, we herein use these stake observations to assess the other forms of accumulation measures including radar and sonic.

2.2 PROMICE

The 'Programme for Monitoring of the Greenland Ice Sheet' (PROMICE, see www.promice.org) was launched by the Danish Energy Agency and is described in detail in [*van As*, 2017]. Among other variables, it provides near-continuous observations of surface radiative fluxes as well as atmospheric standard measurements for 23 stations spread around Greenland's ablation zone. Many of these stations have data reaching back to 2008.

PROMICE data are freely available via www.promice.org. An example of PROMICE data is shown in Figure 2, where the red and yellow areas in the lower left image indicate months/local times, where the infrared-derived surface temperature exceeds zero degrees, indicative of surface melt. Each observation station also measures 'snow height' via sonics mounted roughly 1.5 meters away from the tower. These observations might serve as proxy for snowfall accumulation and are evaluated in detail further down.

NUK_U: 64.51 N, -49.26 E, Elev: 1130 m

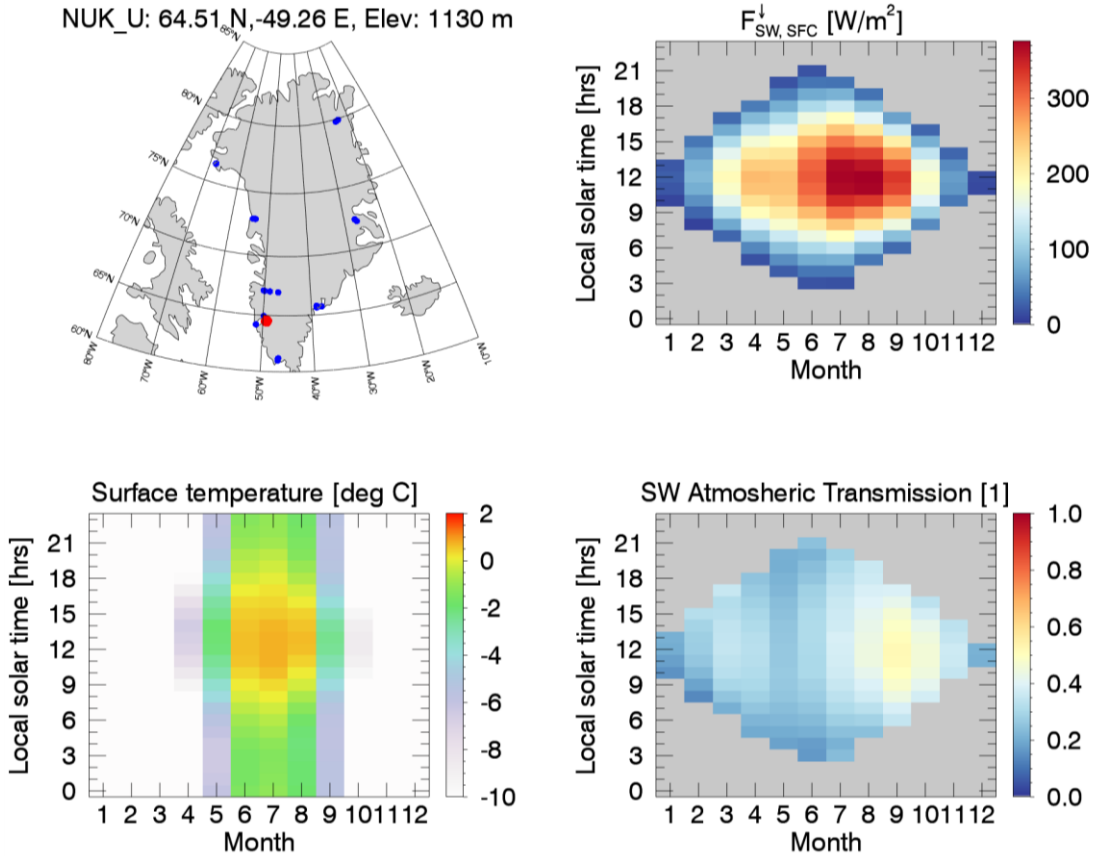


Figure 2: Example observations from PROMICE station NUK_L, corresponding to the red dot in the upper left image. The blue dots in the upper left plot indicate the locations of all other PROMICE stations. The upper right plot shows the observed monthly and hourly averaged shortwave (SW) downward flux at the surface, the lower left plot shows the surface skin temperature derived from observed upwelling infrared surface observations, and the lower right plot shows the SW atmospheric transmission estimated from the SW downward flux at the surface and the incoming solar radiation at the top of the atmosphere. In the lower left plot, yellow to red colours indicate surface skin temperatures above freezing, while white reflects temperatures below -10 °C.

2.3 GC-NET observations

Similar to PROMICE, GC-NET provides long-term observations of atmospheric variables measured near the surface using automatic weather stations. GC-NET data are available from <http://cires1.colorado.edu/steffen/gcnet/>. For details on the data processing and collection, see *Box and Steffen* [2000].

GC-NET data include atmospheric temperature, moisture, wind speed and direction, as well as surface radiative fluxes. In addition, each weather station measures ‘snow height’ via two sonics mounted roughly 1.5 meters away from the tower. Similar to PROMICE, these observations might serve as proxy for snowfall accumulation and are evaluated in detail further down.

2.4 CloudSat observations

CloudSat [Stephens et al., 2002; Stephens et al., 2008] carries the single-frequency W-band (94 GHz) Cloud Profiling Radar (CPR, [Tanelli et al., 2008]). CPR has provided global cloud and precipitation profiles since 2006, however, only daytime scenes can be observed since 2010 due to a hardware failure. The CPR is a non-scanning, near-nadir pointing instrument with a mean spatial resolution of ~ 1.5 km and a vertical range gate spacing of 500 m, although instrument oversampling enables 240 m data bins in the CloudSat data products. In the framework of this study, we use the 2C-SNOW-PROFILE [Wood et al., 2014] together with the GEOPROF reflectivity profiles and ECMWF-AUX temperature and moisture profiles [Stephens et al., 2008]. Product documentation can be obtained from the CloudSat Data Processing Center (<http://www.cloudsat.cira.colostate.edu/>). All analysis is based on the CloudSat Release 5 data, which were made publicly available by the Data Processing Center in June 2018.

Figure 3 shows the number of CloudSat measurements available all over of Greenland (top) and within a 50 km range from Summit Station (bottom). One can clearly identify the reduction in data coverage after the CloudSat battery failure in April 2011. Even after operations were restored, data collection was limited to the sunlit part of the orbit, leading to an annual cycle in the number of observations available over Greenland.

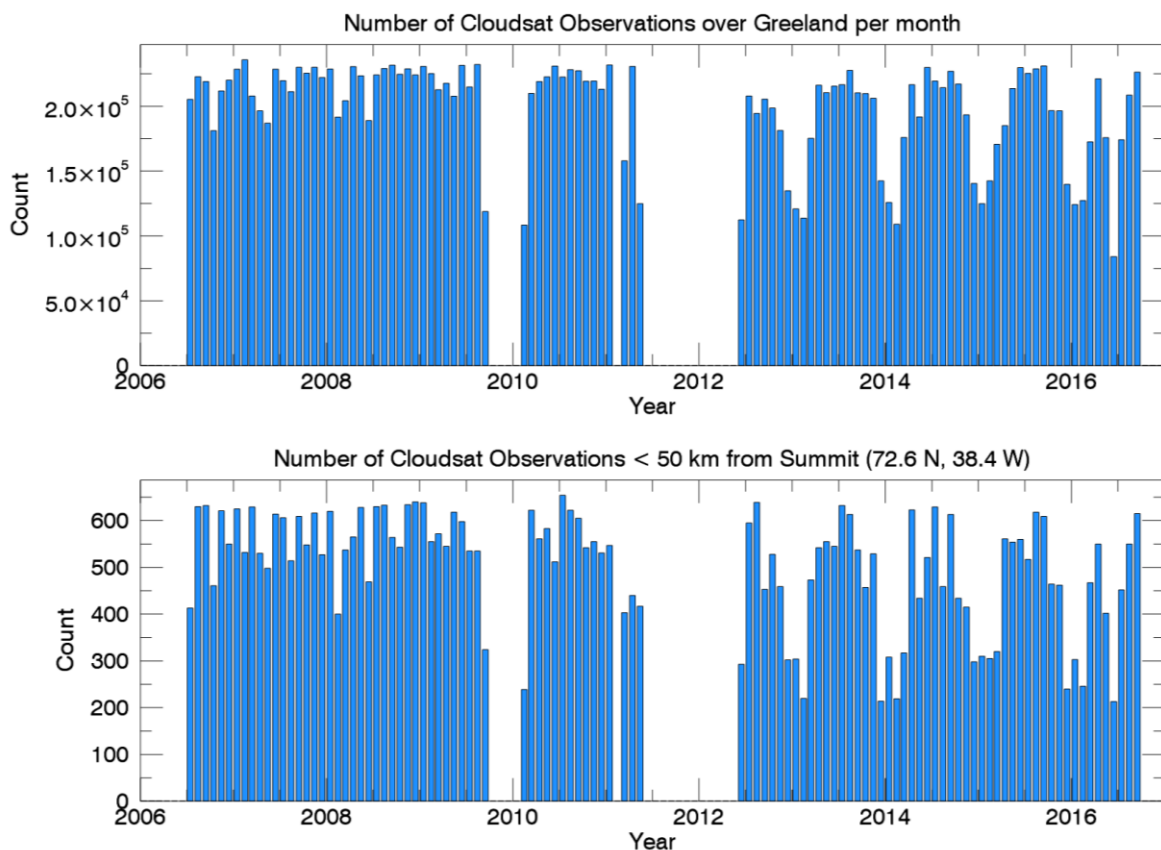


Figure 3: Number of CloudSat observations per month all over Greenland (top) and within 50 km of Summit Station (bottom).

Figure 4 shows the spatial distribution of these measurements over Greenland. Because of CloudSat's 16-day repeat pattern, coverage at high spatial resolution creates a diamond-shaped pattern over Greenland as can be seen in the right panel of Figure 4. This pattern limits the maximum resolution of any climatology based on CloudSat data. At a resolution of roughly 100 x 100 km, the coverage appears more evenly distributed, apart from a north-south gradient which is caused by the higher coverage near the maximum coverage latitude around 81.8 degrees caused by CloudSat's inclination of about 98.2 degrees.

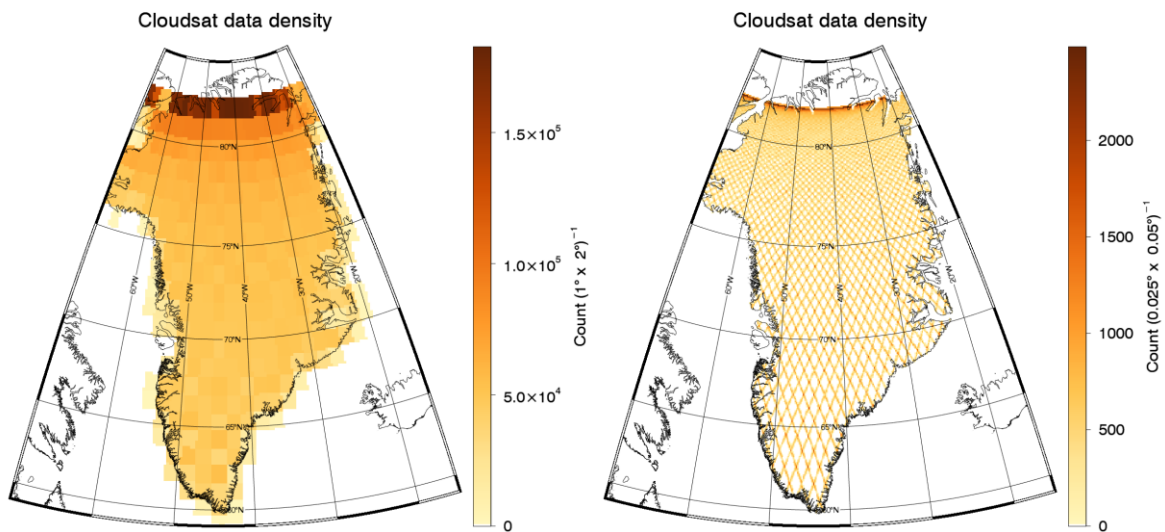


Figure 4: CloudSat data density over Greenland at 1 × 2 degrees (left, approximately 100 km × 100 km) and 0.025 × 0.045 degrees (right, approximately 2.5 km × 2.5 km). Shown is the total number of observations per grid box over the period from 2006 to 2016.

3 Temporal and spatial variability of snowfall over the GrIS

3.1 Temporal variability of precipitation at Summit from ICECAPS

3.1.1 Snowfall accumulation from sonic and stake field

We now compare snowfall accumulation rates from the stake field (see section 2.1) to sonic-derived daily accumulation rates. Summit Station is in an excellent location to make such a comparison as there is no melting that would additionally complicate matters. The observed surface height changes are therefore a result of four distinct processes: snowfall, sublimation, snowpack compression, and snow drift. While the three latter processes clearly contribute to surface height changes, their impact on stake height is minor compared to accumulation by snowfall (see *Castellani et al.* [2015] and references therein).

The resulting snowfall surface heights and accumulations for Summit Station are shown in Figure 5. From the top panel one can identify the snow accumulation derived from the stake field as a smooth black curve. The long-term average height change as observed by the stake field amounts to about 71 cm/year. The variability between the 121 stakes is relatively small with only an about 5% relative deviation in accumulation rates derived for individual stakes (not shown).

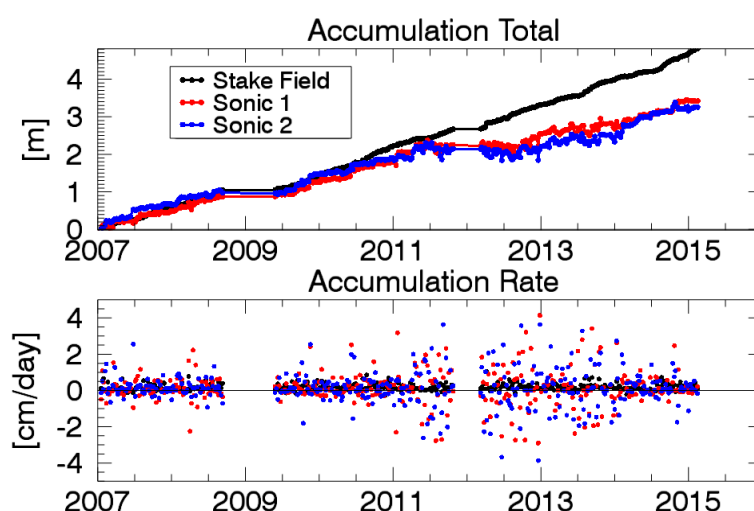


Figure 5: GC-NET sonic derived and stake field derived total accumulation and accumulation rates at Summit Station. There are two sonics operating at each GC-NET station.

For the first part of the time series, roughly up to 2012, the sonic followed the stake field reasonably well, but then significantly underestimated accumulation between about March 2012 and March 2014. In this period, the sonic data is also very noisy as indicated by the large variability of the accumulation rates. The standard deviation of the sonic dataset is 0.95 cm/day and the mean value over all accumulation rates is 0.13 cm/day, thus the standard deviation is about a factor of seven bigger than the mean accumulation rate. For the stake field, we obtain a mean accumulation of 0.18 ± 0.18 cm/day.

For the characterization of snowfall at Summit, we will use the stake field observations as a reference from hereon. In light of a Greenland-wide assessment of snowfall accumulation, these results highlight the importance of quality control for sonic observations. While all GC-NET and PROMICE data are equipped with sonics, the use of these data will require significant quality control efforts. This is addressed further in section 3.3.

3.1.2 Precipitation type

Precipitation is by far the largest source of mass of the GrIS and inter-annual precipitation variability is the main driver of inter-annual variability in the mass balance of the GrIS [van den Broeke et al., 2009]. From a climate perspective, current-day precipitation variability appears highly related to large-scale weather patterns. For example, Seo et al. [2015] have shown that the variability in the North Atlantic Oscillation (NAO) is positively correlated to changes in summer and winter precipitation over the GrIS (but less so for fall and spring). As summertime NAO has decreased over the last about 20 years, Greenland Blocking Index (GBI, high pressure over Greenland, strongly anti-correlated with NAO) has increased in all seasons since 1991, particularly in summertime (June-July-August) [Hanna et al., 2015]. Phases of high GBI are related in general to warmer summer temperatures over the GrIS, less frontal passages, less precipitation over the central and eastern GrIS, and warm, moist air advection over the Davis Strait and the Canadian archipelago [Belleflamme et al., 2015].

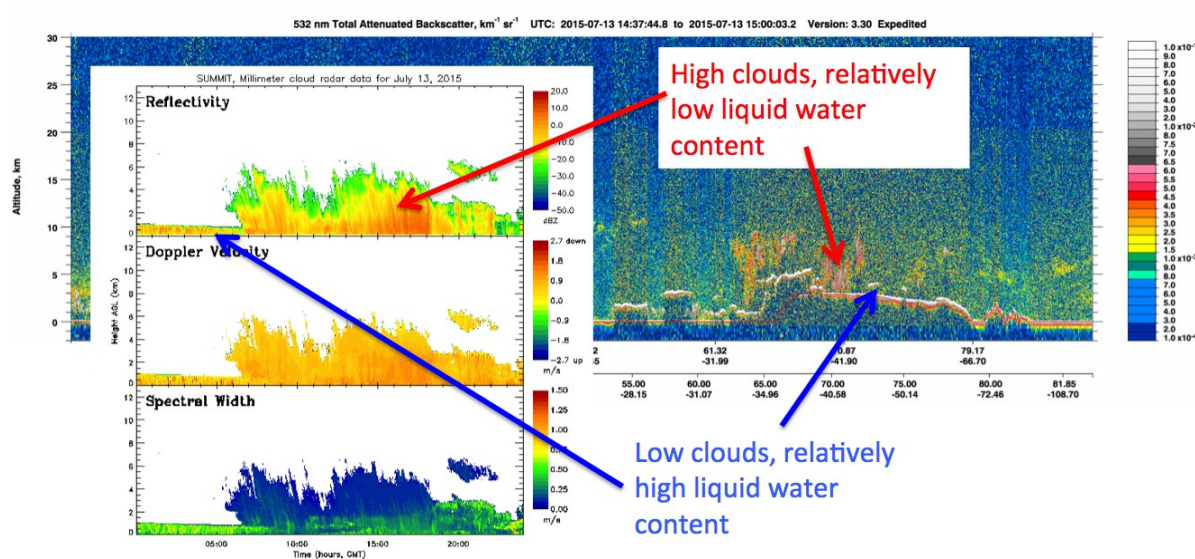


Figure 6: Lidar and radar observations of a high-latitude precipitating weather system on July 13, 2015. The CALIOP lidar observations (with background blue) represent a satellite transect over Greenland. The radar observations are from the ICECAPS MMCR. One can distinguish two different types of precipitation. Precipitation associated with the low clouds (see location of blue arrows) is dominated by riming and diffusional growth of ice particles in a super-saturated environment. Precipitation in the deeper clouds forms largely by pure ice growth processes with little liquid water present (liquid water path known from ground-based collocated upward looking microwave radiometer observations).

Precipitation over the central GrIS also exhibits unique microphysical characteristics owed to high surface elevations as well as to its strong link to large-scale flow patterns. Two different snowfall regimes are frequently observed, sometimes in close vicinity to each other [Pettersen *et al.*, 2017]. Figure 6 provides an example of observed variability in snowfall events:

- One regime characterized by low super-cooled liquid clouds, which generate a steady if very light snowfall.
- The other regime characterized by deeper nimbostratus-like clouds with a vertical extent of several kilometres.

Depending on atmospheric temperatures, these latter clouds carry little to no liquid water over the higher parts of the GrIS. However, they contribute to a similar extent to precipitation accumulation as do thin liquid clouds. Particles falling out of the thicker clouds are typically only very weakly rimed, if little liquid water is present.

Figure 7 shows examples of precipitation size distributions and examples of rimed and pristine particles. At lower surface elevations or generally under warmer conditions, liquid water in nimbostratus-like clouds increases and riming becomes more important. Thus, cold temperatures over large parts of the GrIS limit the availability of moisture, thereby also reducing the relative importance of the liquid phase in precipitation generation. Indeed, using ICECAPS observations, Castellani *et al.* [2015] found that the precipitation amount over Summit does not appear to be strongly linked to cloud liquid water path (LWP).

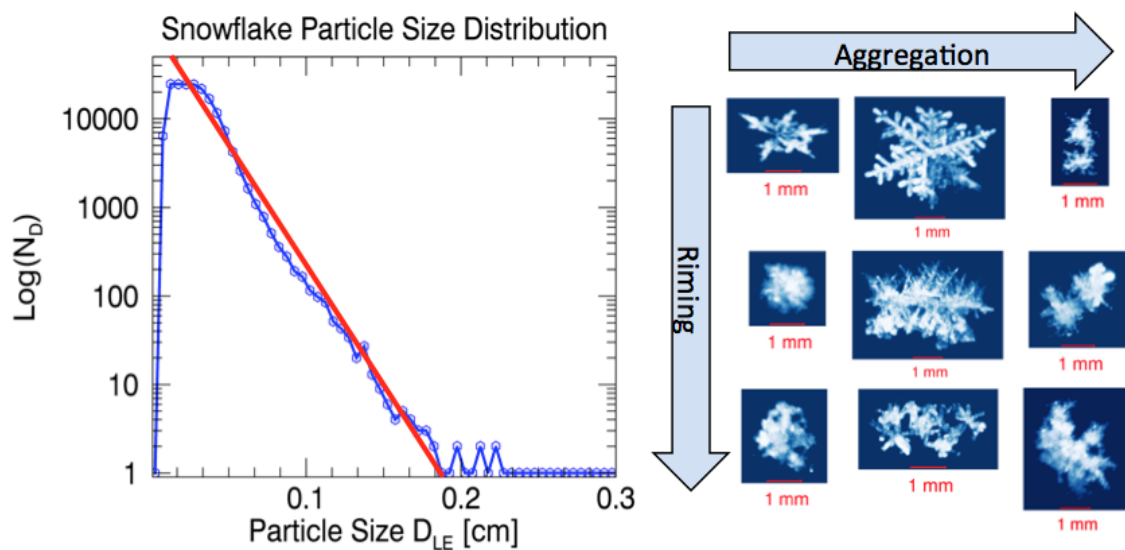


Figure 7: Multi-Angle Snowflake Camera (MASC) ICECAPS-observed surface snowfall size distribution compared to various size distributions typically used in modelling. The data were collected at Summit between June and August 2015. The blue curve shows an observed snowfall size distribution. The red curve is a fit to the size distribution using a combination of exponential relationships (Marshall-Palmer-like). Very small ice particles are not detected by the MASC. The insets show examples observed snowflakes at different stages of riming and aggregation.

3.1.3 Consistency between MMCR and POSS radar observations

In order to address issues of blowing snow that might lead to over- or under-estimation of snowfall rates, it is worthwhile to compare precipitation estimates from POSS (near ground-level) with those from the MMCR (about 135 m above the surface). In a first step, we compared MMCR-derived reflectivities (Z_{MMCR}) with POSS-derived snowfall rates (S_{POSS}). Empirically, we found the following Z-S relation:

$$Z_{MMCR} = 21 S_{POSS}^{0.94} \quad (1)$$

Inverting this equation allows for the derivation of snowfall rates from MMCR. The data underlying this plot as well as the resulting fit are shown in Figure 8. This Z-S relation is slightly different from the one used by *Castellani et al.* [2015], which is $Z = 56 S^{1.2}$ and produces somewhat higher snowfall accumulations at the low end of reflectivities. This latter Z-S relation is based on the work of *Matrosov* [2007] and assumes dry mid-latitude snowfall.

We find that our so-derived snowfall rate from MMCR shows a correlation of 0.85 compared to POSS and zero bias (the latter by virtue of regressing MMCR against POSS in the process of generating the Z-S relation.) *Note, that this Z-S relation does not in itself add information beyond a mere consistency check between POSS and MMCR.* However, due to the height of the MMCR observation (135 m above surface), we can exclude drifting snow as a major issue when POSS data is observed. If the POSS was affected strongly by drifting snow, inconsistencies between POSS and MMCR would be expected at the high end of observed radar reflectivities of snowfall rates.

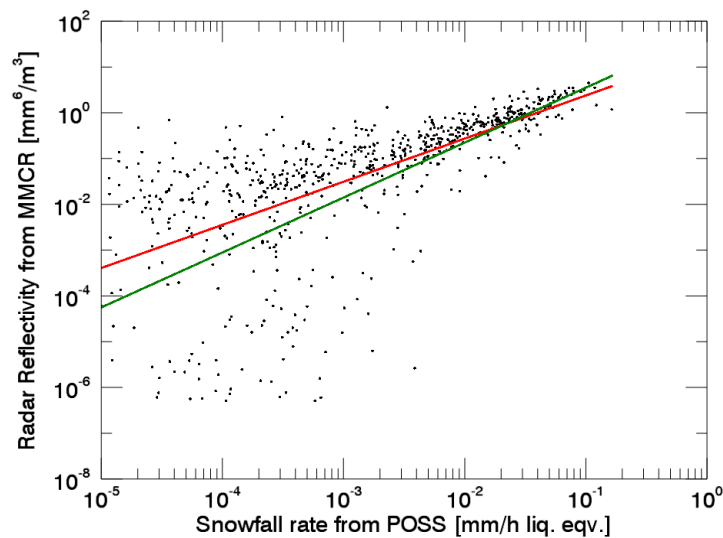


Figure 8: POSS-derived snowfall rates versus MMCR-derived radar reflectivities. The red line corresponds to the Z-S relation shown in Equation (1). The green line corresponds to the Z-S relation used in *Castellani et al.* [2015]. Each dot corresponds to a daily mean snowfall rate.

The results presented so far are consistent with *Castellani et al.* [2015]. In their paper, they further find large discrepancies between radar-derived snowfall rates and snowfall accumulation from ground-based observations, namely a significant underestimation of snowfall accumulation if the above radar observations and Z-S relations are used and reasonable assumptions about the density of the surface snow layer are being made. They speculate that the Z-S relations used might not be appropriate for the type of snowfall observed at Summit. Indeed, often snowfall at Summit consists of very small particles with little riming and only moderate aggregation. Particle sizes rarely exceed two millimetres and by far the most particles are below one millimetre. In the following section we address the impact of different choices of Z-S relations on the radar-derived precipitation estimates.

3.1.4 Radar-derived precipitation – impact of Z-S relation

In order to further understand the impact of particle habit on radar-derived snowfall rates and possible implications on accumulation estimates, we use the MMCR-observed radar reflectivities and apply different published Z-S relations (Table 2). In addition to the M07 relation used in various previous studies, we employ two Z-S relations proposed by [*Kulie and Bennartz, 2009*] that apply to single habits, which based on the above considerations and observations might be better proxies for snowfall at Summit than M07.

Table 2: Parameters of Ka-band (MMCR) and W-band (CloudSat) Z-S relations used in this study. The POSS operates at X-band so that the Z-S relation is not directly comparable the Z-S relations for MMCR.

Name	A (Ka-band)	B (Ka-band)	A (W-band)	B (W-band)	Reference
M07	56.0	1.20	10.0	0.80	[<i>Castellani et al., 2015; Matrosov, 2007; Pettersen et al., 2017</i>]
KB09_LR3	24.0	1.51	13.2	1.40	[<i>Kulie and Bennartz, 2009</i>] using [<i>Liu, 2008</i>] 3-bullet rosettes
KB09_HA	313.3	1.85	56.4	1.52	[<i>Kulie and Bennartz, 2009</i>] using [<i>Hong, 2007</i>] aggregates
L08	---	---	11.5	1.25	[<i>Liu, 2008</i>]
HI11_L	---	---	7.6	1.30	[<i>Hiley et al., 2011</i>]
HI11_A	---	---	21.6	1.20	[<i>Hiley et al., 2011</i>]
HI11_H	---	---	61.2	1.10	[<i>Hiley et al., 2011</i>]
POSS	N/A	N/A	---	---	[<i>Pettersen et al., 2017; Sheppard and Joe, 2008</i>]
MMCR-POSS	21.0	0.94	---	---	Fitted MMCR to POSS. See section 3.1.3

In Figure 9, we compare liquid equivalent snowfall accumulation derived from MMCR and POSS with the actual geometric accumulation obtained from the stake field. The ratio between the two quantities is the effective density of the snowpack that is needed to explain the actual accumulation via the liquid equivalent snowfall rates.

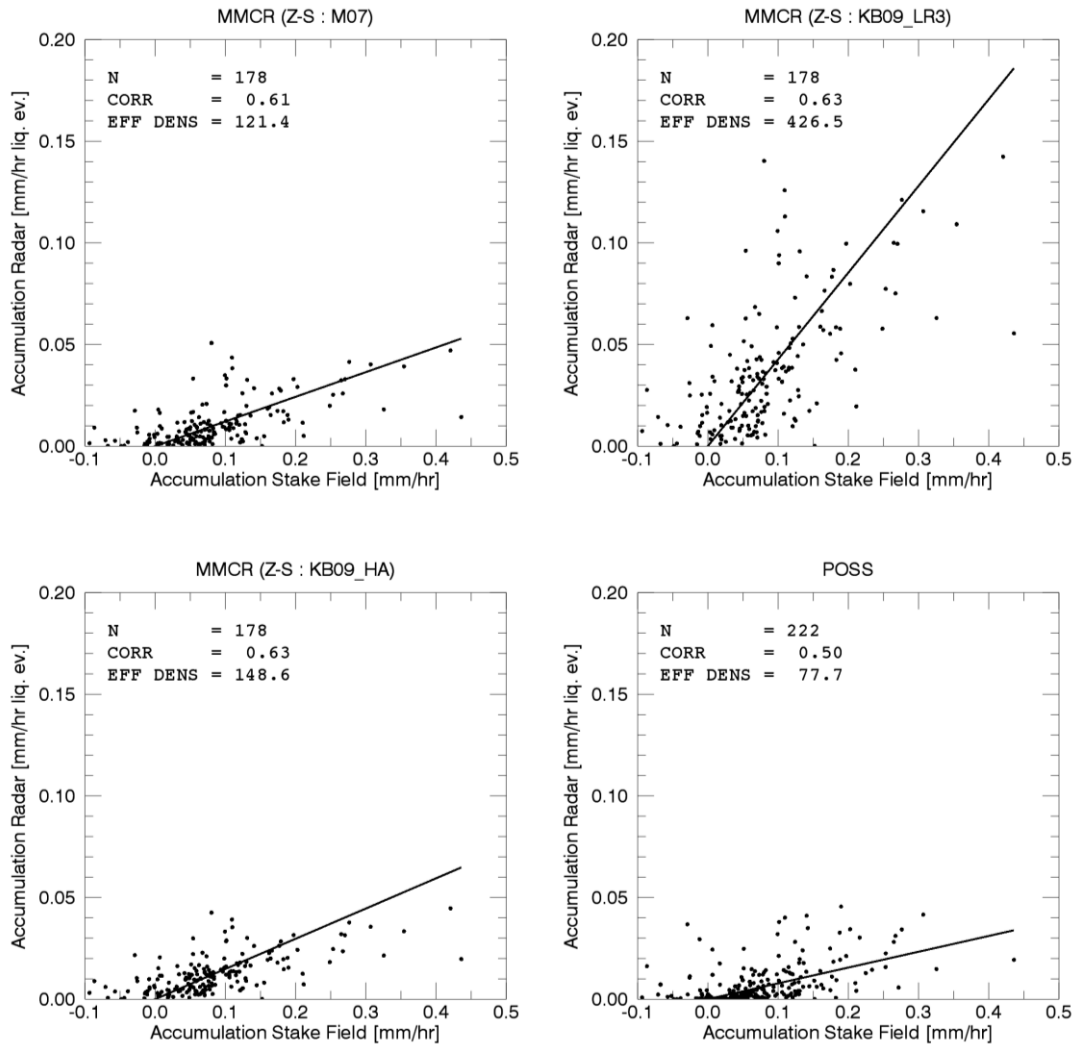


Figure 9: Comparison between snowpack accumulation rates from stake field and MMCR-derived or POSS-derived liquid equivalent accumulation rates. ‘EFF DENS’ is the effective density in [kg/m³] of the snowpack needed to explain the mean stake accumulation by the liquid equivalent precipitation from either MMCR or POSS. The lines start at [0,0] and have the reported effective density (divided by 1000) as slope. Each data point corresponds to one week of observations as the snow stake heights are read of typically once a week.

One can see that between the different Z-S relations used, most yield an effective snowpack density around 100 kg/m³. Only KB09_LR3 yields a significantly higher effective density of 426 kg/m³. As already pointed out by *Castellani et al.* [2015], observed densities in the upper snow layers at Summit are in the order of 300-450 kg/m², so that it appears KB09_LR3 yields more realistic snowfall accumulations than the other Z-S relations. KB09_LR3 would be consistent also with the type of snowfall often observed at Summit, that is mostly individual ice crystals with little aggregation or riming. We note that KB09_LR also performed among the best for a series of studies using CloudSat’s W-band radar [*Hiley et al.*, 2011; *Kulie et al.*, 2010]. These results indicate that KB09_LR3 would possibly be a better choice for a Z-S relation at Summit than M07.

Figure 10 provides estimates of the annual cycle of monthly liquid equivalent snowfall derived from both POSS and MMCR. Based on the above discussion, it is likely that the POSS underestimates total snowfall and that the MMCR with KB09_LR3 applied provides more realistic estimates. The annual snowfall total based on MMCR is 275 ± 65 mm/y, where the uncertainty reflects interannual variability in the five-year period. Consistent with *Castellani et al. [2015]*, the highest snowfall rates are observed during the summer months, where average liquid equivalent accumulation can be between about 10 mm and 30 mm per months. In contrast to their earlier study however, we find somewhat lower values of accumulation.

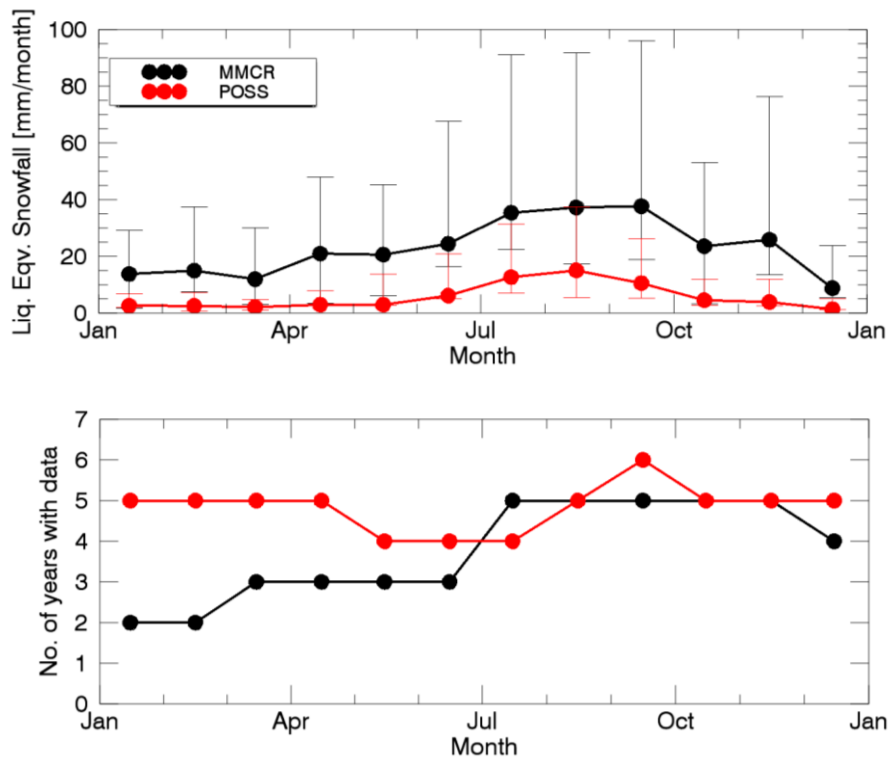


Figure 10: The upper panel shows the POSS and MMCR-derived monthly mean liquid equivalent snowfall accumulation at Summit for the years 2010-2015. For MMCR the Z-S relation KB09_LR3 was used. The associated error bars give the minimum and maximum monthly mean values found over that same period. The lower plot shows how many years contributed to the upper plot for each month.

3.2 Evaluation of the use of space-borne radar for precipitation studies

Here we assess the full CloudSat snowfall dataset over Greenland in terms of its viability for climatological snowfall studies. Amount and spatial distribution of the data used for this assessment are shown in Figure 3 and Figure 4. We analyse the dataset with respect to the following issues:

- a) Effects and removal of ground clutter.
- b) Impact of height of CloudSat observation above the surface.
- c) Impact of Z-S relation.

At Summit, concomitant observations from stake field and MMCR allow for a detailed assessment of these issues. Based on this analysis, we provide a best estimate of snowfall over the GrIS, which is then compared to the PROMICE and GC-NET surface stations in section 3.3.

3.2.1 Effects and removal of ground clutter

CloudSat observations in the lowest range bins above the surface are affected by ground clutter. Because of topography, this effect is more pronounced over land than over ocean. The CloudSat SNOWPROF product accounts for the effects of ground clutter by providing a confidence flag for the retrieved surface snowfall rates. This flag depends on the type of surface as well as on other criteria, such as vertical consistency of retrieved snowfall rates. A key input over the highly structured coastal terrain of Greenland and the fringes of the GrIS is the height of the surface bin, which describes where the radar beam first interacts with the surface. This quantity is provided in the CloudSat data and is retrieved from the radar reflectivity itself as well as from an underlying digital elevation model.

In our analysis, we found that the height of the surface bin is not always accurately represented over Greenland. This occasionally causes significant outliers in retrieved surface snowfall rate. To study and possibly correct for this issue, we use the IceBridge BedMachine (V3) surface topography [Morlighem *et al.*, 2017] and collocate those with each individual CloudSat observation. We then re-derive snowfall rates based on the 5th radar bin above the surface as defined by this new topography. We compare those retrievals to the originally retrieved snowfall rates, which also typically are taken from the 5th radar bin above the surface, but with a different surface elevation model defining the surface. We restrict our analysis to SNOWPROF confidence flag values 3 and 4, which indicate high confidence in the retrieval.

The difference in elevation reported between the CloudSat and BedMachine topographies can be seen in Figure 11. It is not entirely unrealistic that some of the observed differences are caused by melting in the ablation zone. However, differences might also be caused by other factors. Clearly, some of the coastal regions with the highest differences experience significant amounts of snowfall. The effect of using different underlying surface topographies for snowfall retrieval and accumulation is shown in Figure 12 to Figure 14.

Figure 12 shows two-dimensional histograms of radar reflectivity and derived SNOWPROF surface snowfall rate. For each reported snowfall rate, the corresponding radar reflectivity was obtained from the corresponding CloudSat GEOPROF product. The left panel of Figure 12 shows the surface snowfall rate and reflectivity reported directly from the product. The right panel shows the revised snowfall rate

accounting for the BedMachine topography. Note that for the right panel all snowfall rates are also directly retrieved from SNOWPROF. In contrast to the left panel however, the snowfall rates are occasionally taken from radar bins higher in the atmosphere to account for the higher topography estimates from BedMachine.

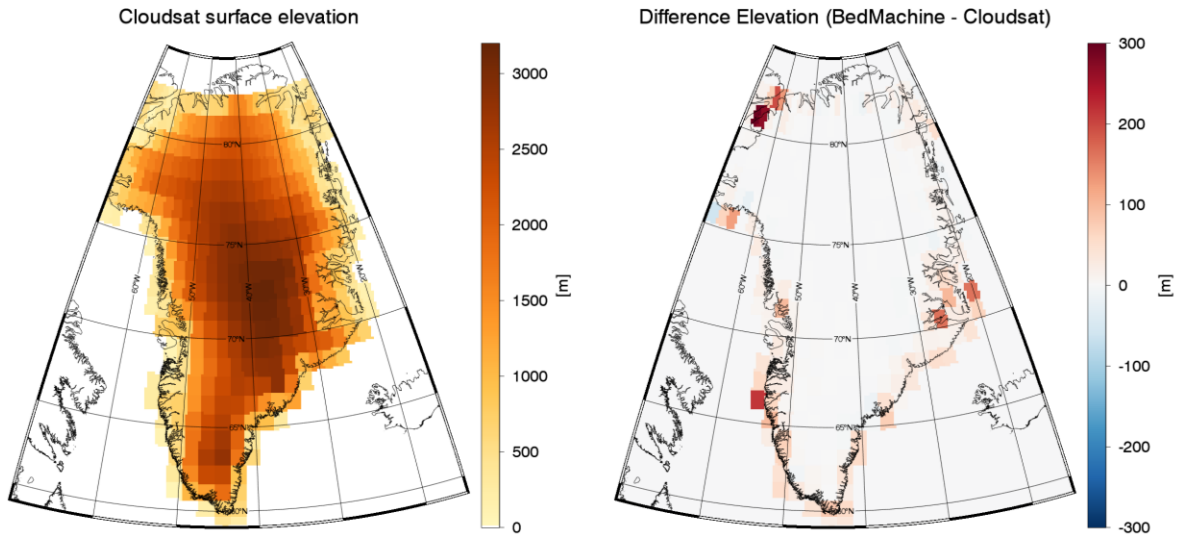


Figure 11: The left panel shows the mean elevation reported from CloudSat binned to 1×2 degrees. The right panel shows the elevation difference between IceBridge BedMachine v3 [Morlighem et al., 2017] and CloudSat. Note, that open water and sea ice observations are excluded from the dataset, so that differences observed near the coast only stem from ice-free land or GrIS observations within each grid box.

Comparing the panels in Figure 12, we note that there is a significant number of high reflectivities associated with very high and often physically implausible snowfall rates of up to 50 mm/h (upper right part of left panel of Figure 12). Using the BedMachine topography eliminates these high snowfall rates. A visual inspection of a few of these cases also indicates that these were clutter-affected observations in the original CloudSat product, which are successfully eliminated using the BedMachine topography. The revised formulation for the lowest valid CloudSat bin above the surface thus leads to a significant reduction of surface clutter as shown in Figure 12.

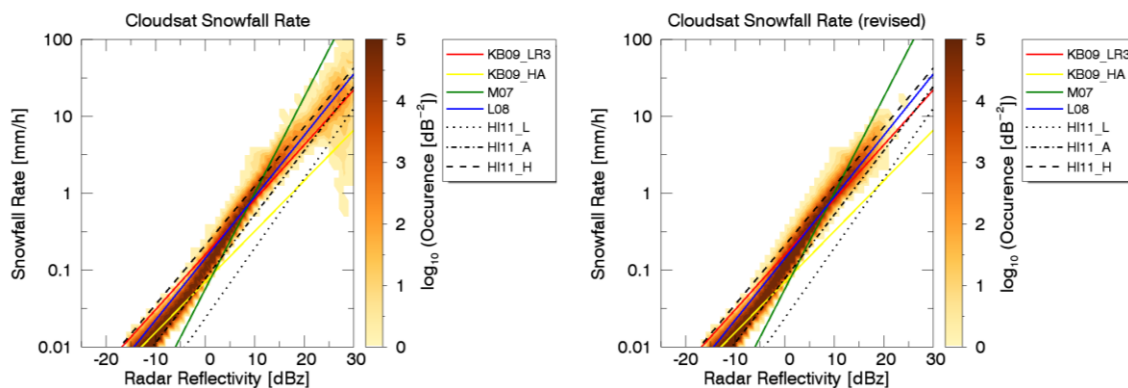


Figure 12: Histogram of occurrence of snowfall rate versus radar reflectivity for the entire CloudSat dataset over Greenland. The left panel shows the relation if the SNOWPROF surface snowfall rate is used face value. The right panel shows the relation with corrected topography. Different Z-S relations are shown as well.

The effect of the above revisions can be seen in Figure 13, which shows the actual heights of CloudSat “surface snowrate” observations above the surface as well as the difference between the original SNOWPROF heights and the revised heights. One can see that in the original formulation, the distance to the surface near the coast is often in the 1000 m range which would likely lead to ground clutter [Maahn et al., 2014], given the structured terrain. Note that Figure 13 shows the effect of the correction on the height of the lowest valid CloudSat observation above the surface (whereas Figure 11 only shows the difference between two topographies). The effect of these differences in topographies (Figure 11) is amplified as CloudSat observations are binned at 240 m vertical resolution. Because of this 240-m-binning slight changes in height observed in Figure 11 can result in the larger changes in CloudSat observation height observed in Figure 13 (e.g. a difference in topography of 50 m might lead to the lowest valid CloudSat bin getting pushed up by 240 m).

Over the central GrIS, the average observation height is not affected. We have examined this for the 1×2 degrees grid box around Summit, where typically the 5th radar bin above the surface is selected (around 1200 m above the surface). In general, it is important to bear in mind that CloudSat “surface snowrate” observations over structured terrain typically come from about 1200 meters above the surface and thus do not observe precipitation processes below that altitude. The impact of this for the high GrIS is studied in Section 3.2.2.

Figure 14 shows the integrated effect of the ground clutter artefacts in the CloudSat surface snowfall rates on accumulation. The grand mean snowfall rate over all CloudSat data over Greenland would be approximately 0.225 mm/h in the revised formulation. Not correcting for artefacts reduces the grand mean by 15 % to about 0.2 mm/h but with significant contributions from larger than 20 dBz, which are eliminated when the IceBridge BedMachine surface topography is applied. Observations that were corrected for ground clutter contribute toward the total snowfall at lower reflectivities thereby increasing retrieved snowfall rates between +5 and +15 dBz and increasing snowfall rate in this dBz interval. Note, that Figure 14 only presents the grand mean of all snowfall rates. Because of the large

differences in surface elevation between CloudSat and BedMachine near the coasts, the impact of artefacts in coastal areas will be much higher, when snowfall climatologies are reported. In contrast, these artefacts will not play a major role on the higher part of the GrIS.

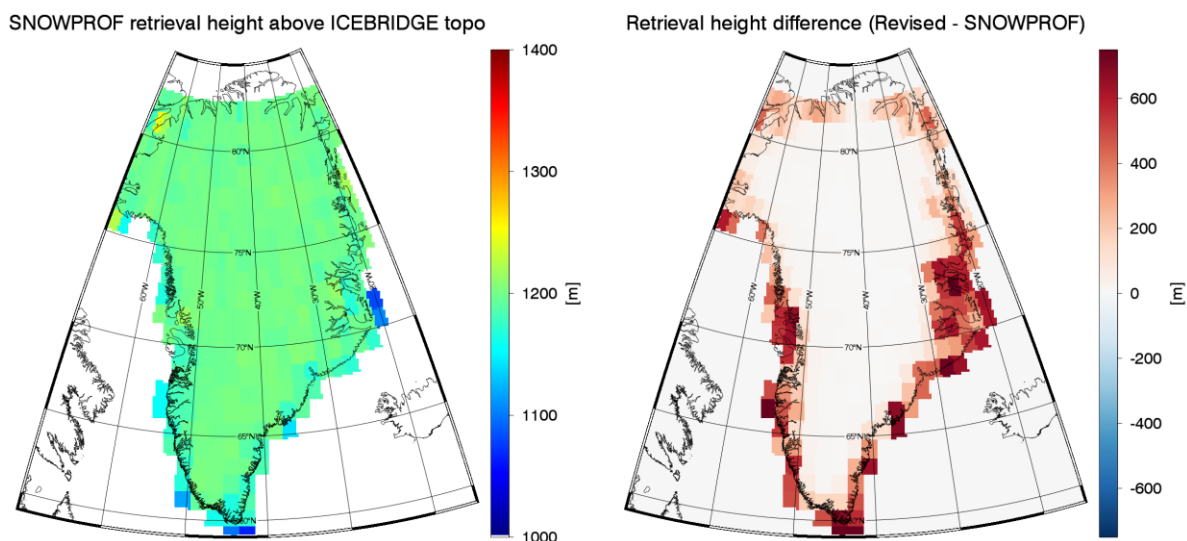


Figure 13: The left panel shows the height of the CloudSat SNOWPROF ‘surface snowrate’ observation above the local topography (from IceBridge BedMachine). The right panel shows the difference between the height used in the revised product and original height. For example, at the southern tip of Greenland, the ‘surface snowrate’ reported in the SNOWPROF product comes from an actual altitude of about 1000 m above the surface. In the revised formulation discussed in the text, this height is pushed up by 500 m to 1500 m.

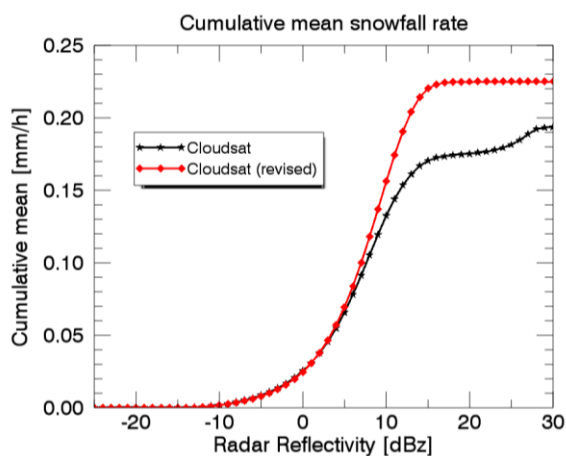


Figure 14: Impact of surface topography issues on cumulative snowfall rates.

Based on the results reported in the current section, we will from hereon only use the revised snowfall rates that are based on the IceBridge BedMachine surface elevation and discard the surface snowfall rates reported in the SNOWPROF product. We note again that the revised surface snowfall rates we

use here are also available in the SNOWPROF product, but are occasionally, mostly near the coasts, taken from higher radar bins than the original surface snowfall rates to avoid clutter artefacts that would otherwise be present.

3.2.2 Impact of height of observations above ground on estimated surface snowfall rate

As shown in Figure 13, CloudSat snowfall observations over Greenland stem from altitudes of around 1200 m above the surface to avoid ground clutter issues. This of course might cause several issues because any precipitation processes happening at lower altitudes are not observed and, consequently, not accounted for in CloudSat estimates.

Here we use MMCR observations from Summit to study the difference between observed reflectivities at an altitude of 1200 m and closer to the surface (135 m). We first average the vertical reflectivity profile of the MMCR between 1000 m and 1500 m to account for the lower vertical resolution of CloudSat. After converting the averaged reflectivity back into dBz units, we compare it with the MMCR reflectivity observed at 135 m above the surface. This comparison is shown in the left panel of Figure 15. One can see that in most cases, the reflectivity observed at CloudSat height is lower than the reflectivity near the surface, possibly owed to precipitation processes occurring at altitudes below 1000 m. There are also cases where the upper reflectivity is higher than the reflectivity near the surface. Cases for such events could include non-precipitating clouds around 1200 m or ice particles sublimating before they reach the surface. These cases might also include situations where the lowest MMCR radar bin might get saturated under high reflectivities (see *Castellani et al.* [2015]). Our own analysis of this saturation effect shows 0.3 % of the MMCR observations to be affected by it with only a vanishing effect on the MMCR snowfall rates reported here. The correction developed in the following paragraph is also not affected. We therefore ignore this saturation effect.

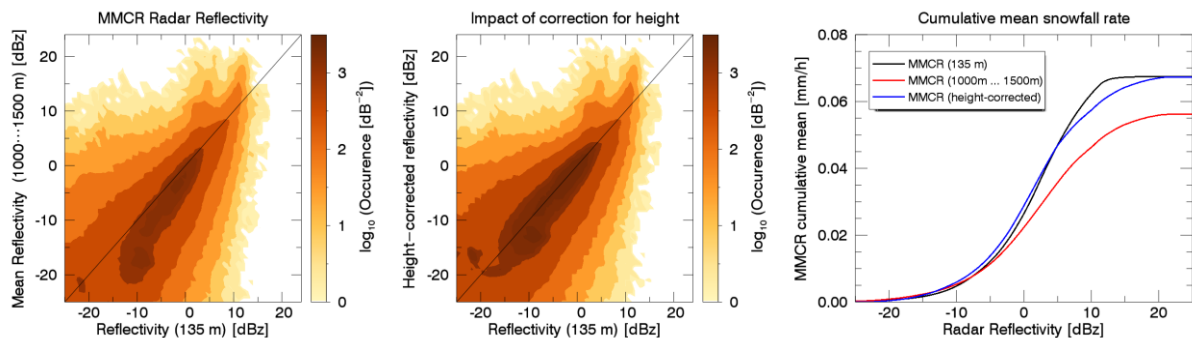


Figure 15: The two left panels show histograms of MMCR observations at Summit. The left panel compares radar reflectivity at 135 m above the surface with the average radar reflectivity between 1000 and 1500 m above the surface, which corresponds to the height range where CloudSat observations are obtained. The middle panel shows a similar plot but with a height correction applied. See text for details. The right panel shows cumulative mean snowfall rates for the different radar reflectivities show in the left and middle plot.

Applying the KB09_LR3 Z-S relation (see Table 2), the red and black curves in the right panel of Figure 15 show the impact of the differences in reflectivity on total cumulative snowfall at Summit. The on average lower reflectivity at 1000-1500 m yields to an under-estimation of the snowfall rate of about

20 % compared to using the reflectivity near the surface. Most of this difference is accumulated in a reflectivity range between -10 and +5 dBz.

In order to correct for this effect, we applied an ad-hoc correction that statistically accounts for this effect:

$$dBz_{corrected} = dBz_{1000...1500} + \left[(1 - 0.2 \cdot \mathbb{1}_{dBz_{1000...1500} > 0}) \right] \quad (2)$$

This statistical correction produces the joint histogram shown in the middle panel of Figure 15 and, by design, matches the total cumulative snowfall near the surface (see blue curve in right panel of Figure 15). The correction drops to zero at 5 dBz, thus does not affect reflectivities higher than 5 dBz. While providing higher corrections for very low reflectivity values, those affect snowfall accumulation only very weakly. E.g. for an observed reflectivity of -30 dBz, the correction is +4 dB leading to a corrected reflectivity of -26 dBz, which still does not produce any significant snowfall.

There are caveats to this correction. Importantly, it will only work if the actually observed atmospheric state is statistically similar to the one on which it was derived. Since the data used for the correction stems from Summit, we expect this correction not to produce viable results outside the higher GrIS. In order to highlight this limitation, we show in Figure 16 the same analysis, but for Barrow, Alaska. As one can see, the application of the correction outlined in Equation (2) has no effect on the snowfall rate. This is simply because at Barrow, snowfall is produced under different atmospheric conditions. The application of the correction also does not deteriorate the results at Barrow because it has, by design, little to no effect on higher reflectivities. This point is important as toward the GrIS ablation zone and in Greenland's coastal regions, one can expect atmospheric conditions to be more similar to Barrow than to Summit.

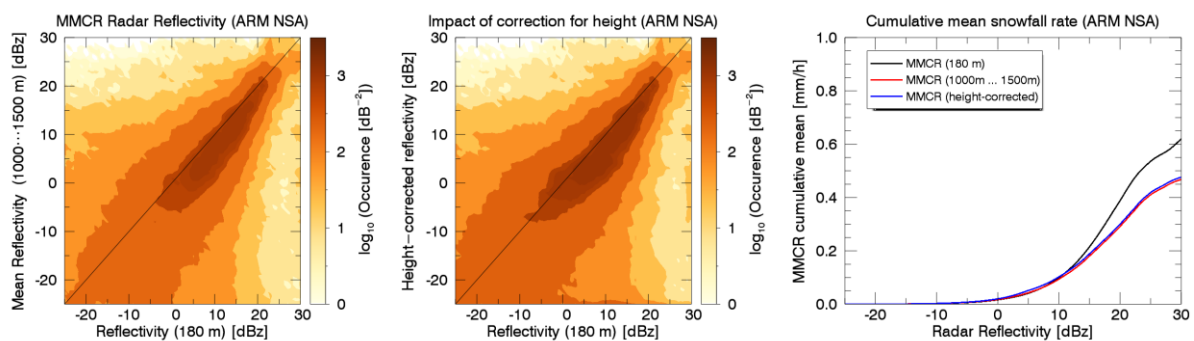


Figure 16: Same as Figure 15 but for the DOE-ARM site at the North Slope of Alaska (NSA) at Barrow, Alaska. The figures are based on 1.08 million radar profiles obtained between 01/2008 and 4/2011. Only data for the winter months November through April are shown. The Barrow MMCR data were obtained from <https://www.archive.arm.gov/discovery/>.

Results presented in Figure 15 and Figure 16 apply to the MMCR, which operates at Ka-band. However, we wish to apply this relation to CloudSat, which is a W-band radar. Z-S relations between Ka-band and W-band are different, because medium-sized ice particles enter the Mie-scattering

region at a smaller size at W-band than at Ka-band. As snowfall rate increases, the difference between W-band and Ka-band typically increases because the number of large particles outside the Rayleigh scattering region will increase at W-band. This leads to a different slope of the Z-S relations at W-band and Ka-band, which might affect the correction proposed here. The Z-S relations for the two bands are shown in Figure 17 for KB09_LR3. For other Z-S relations, depending on the ice particles used and, in particular the underlying size distribution, these differences can be much larger. However, as discussed below, KB09_LR3 is probably more representative for the light snowfall observed over the high GrIS than other Z-S relations, which apply more to the mid-latitudes. From Figure 17, one can identify the slight difference in slope between Ka-band and W-band. However, since the above-proposed correction only has significant effect in the range between -10 dBz and +5 dBz, the effect of the earlier onset of Mie-scattering in W-band than in Ka-band will be very small.

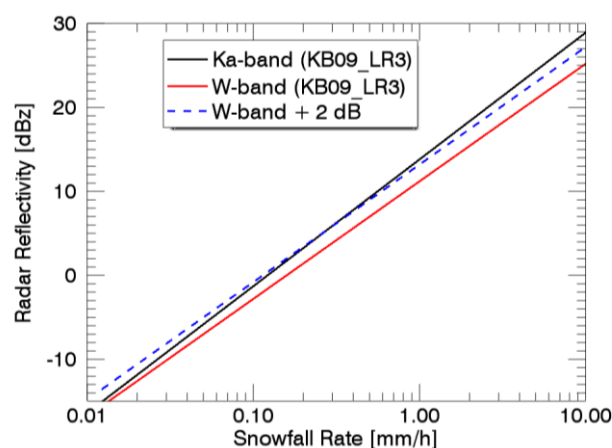


Figure 17: Radar reflectivity at Ka-band (MMCR) and W-band (CloudSat) as function of snowfall rate for KB09_LR3 Z-S relation. The blue dashed curve has the same slope as the red curve and is shown only as a visual reference to see the slight difference in slope between the red and black curves.

Based on this discussion, we will apply the above-formulated correction to CloudSat observations without further modification for radar wavelength. This will affect the retrieved snowfall estimates over the higher GrIS but will have little effect on estimates in the ablation zones near the coast where snowfall is expected to be associated with higher reflectivities. In future studies, it would be interesting to look at this issue further and study for example potential temperature dependencies. Initial results from Summit do show a weak dependency of the correction on surface temperature (not shown). We have also tested for a dependency on precipitation type using the classification by *Pettersen et al.* [2017], but did not find any significant differences in the correction between their IC (ice-only cloud) and LWC (liquid-water containing) clouds. However, expanding this analysis to more Arctic sites, such as Barrow, might likely allow for a more general correction that might help mitigate some of the issues related to the height above surface of CloudSat snowfall estimates.

3.2.3 Impact of Z-S relation

Figure 18 shows cumulative snowfall rates based on the full CloudSat dataset in a similar manner as Figure 14. The original CloudSat SNOWPROF optimal estimation retrieval as well as L08 and KB09_LR3

and M07 are relatively similar in their results (to within $\pm 10\%$). All other Z-S relations fall outside that range. The right panel of Figure 18 shows the impact of the height-correction (previous section) on the retrieval, which by example of the 'KB09_LR3' relation increases cumulative snowfall rate near 30% at around 0 dBz and 7% at around 30 dBz (difference between red curves between the left and the right panel). Note that for the original SNOWPROF CloudSat retrieval this correction cannot be applied, as the original retrieval is an optimal estimation retrieval that cannot simply be re-calculated with revised reflectivities.

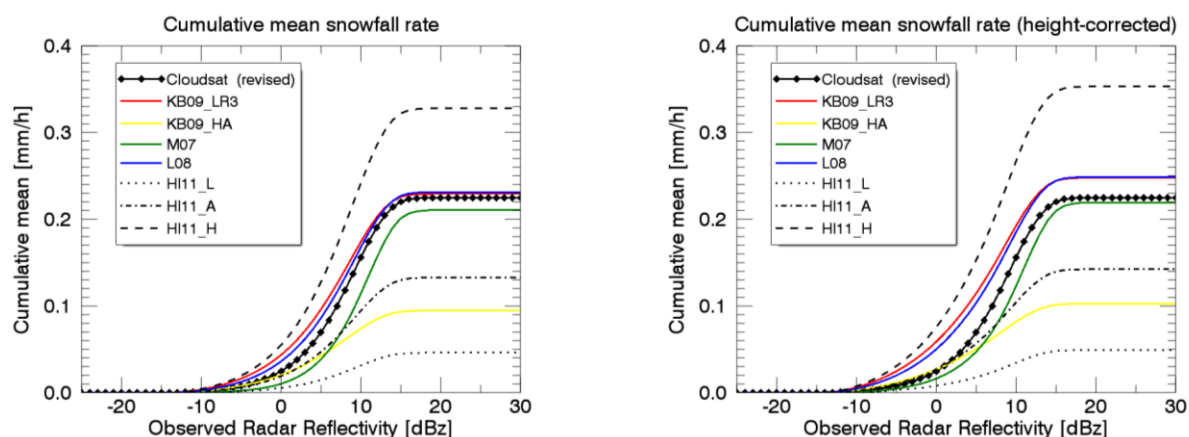


Figure 18: Cumulative snowfall rates derived from all CloudSat observations over Greenland. The thick black line corresponds to the CloudSat-derived surface snowfall rate from SNOWPROF with ground-clutter removed ('revised', same as in Figure 14). The other lines correspond to the Z-S relations applied to CloudSat reflectivities without height correction (left panel), and with height correction (right panel).

Figure 18 also highlights the importance of low detectability thresholds for space-borne precipitation radar, if GrIS snowfall is to be observed. About 50% of the total accumulation occurs at reflectivities between -10 dBz and +7 dBz. A minimum radar detectability threshold should therefore be lower than -10 dBz.

3.2.4 Comparison against stake field

To compare CloudSat observations with the stake field, we selected all CloudSat data (height- and clutter-corrected) within 50 km from Summit and averaged them over the time intervals between stake field observations, which are typically read off in weekly intervals. We rejected any match-ups where there were less than 30 CloudSat observations within a given stake field time interval. This resulted in 369 pairs of weekly accumulation statistics from CloudSat and concurrent stake field observations over the period 2007-2016.

Figure 19 shows the accumulation rates obtained from CloudSat compared to the stake field for those 369 data points for different Z-S relations. Compared to the corresponding figure for MMCR (previous section) correlations are much lower. This increased scatter is not surprising given that CloudSat provides only one to three orbits per week around Summit. However, in terms of total accumulation over longer time periods, CloudSat does show a good agreement with the stake field as can be seen in Figure 20. We note that the good agreement of the total accumulation seen in Figure 20 is by design,

as the effective density is used to scale the Cloudsat observations to the stake field. However, the curves follow each other closely over the entire observation period, which could not necessarily be expected if, for example, CloudSat would preferably sample certain types of snowfall. This is despite the large scatter between CloudSat and the stake field seen in Figure 19. This scatter can partly be explained by CloudSat not being perfectly collocated in space and time with the ground-based observations and by relatively few individual CloudSat overpasses contributing to each weekly average. Often CloudSat might miss an individual snowfall event and hence report a near-zero snowfall rate. In other cases, CloudSat might observe a single snowfall event which is not representative for the entire week and thereby over-estimate the weekly snowfall. Both effects can be observed in Figure 19.

Similar to the above discussion on MMCR, choosing an appropriate Z-S relation remains critical in terms of the effective density needed to transfer CloudSat liquid equivalent snowfall rates to accumulation rates. The four Z-S relations shown in Figure 19 provide effective density values between 181 and 365 kg/m³, providing a generally better agreement with the numbers of 240-380 kg/m² discussed in Section 3.1.4. The three Z-S relations ('HI11_H', 'KB09_LR3', and 'L08') produce a mean value of 298 kg/m².

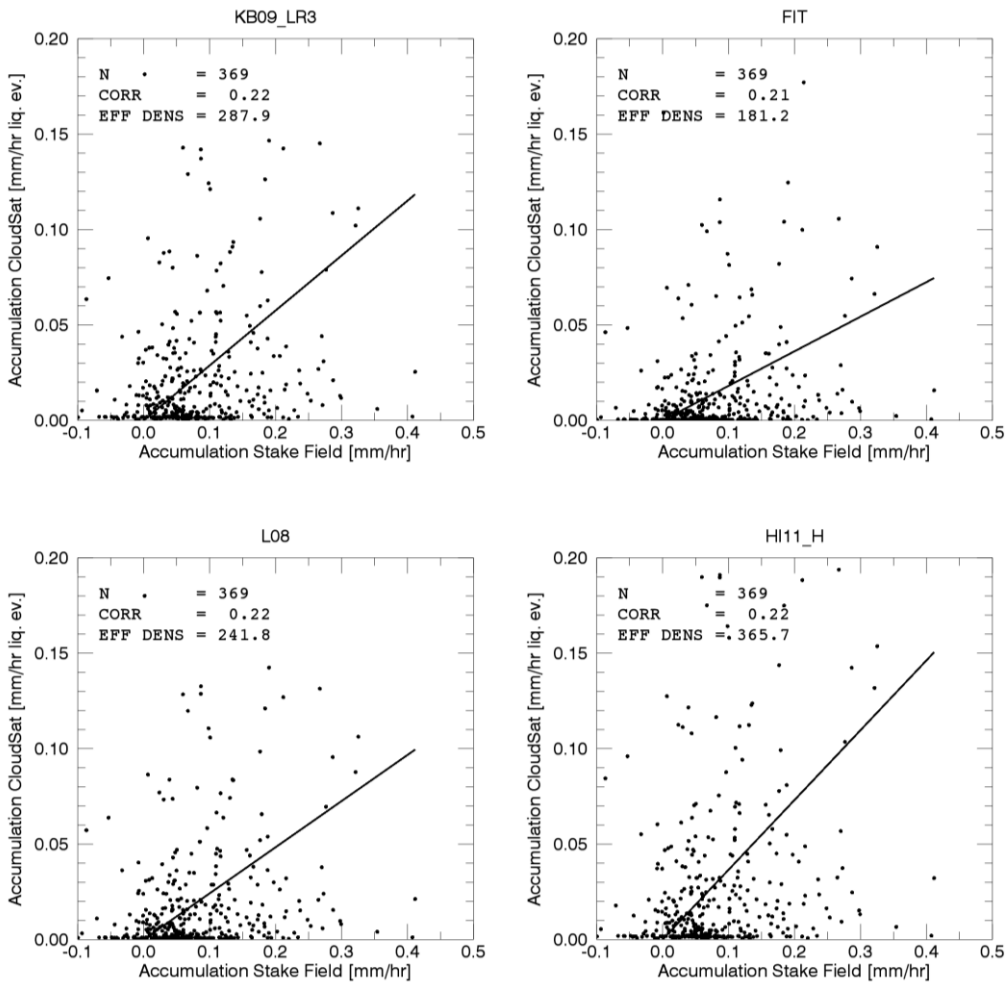


Figure 19: Same as Figure 9, but for CloudSat versus stake field.

Figure 20 shows the accumulation at Summit between 2007 and 2016 based on all 369 weeks where concurrent CloudSat observations were available and using the effective densities reported in Figure 19 for the three different Z-S relations. Total accumulation based on these estimates is about 65 cm/yr derived from the 4.75 meters of accumulation seen in Figure 20 over the 369 weeks.

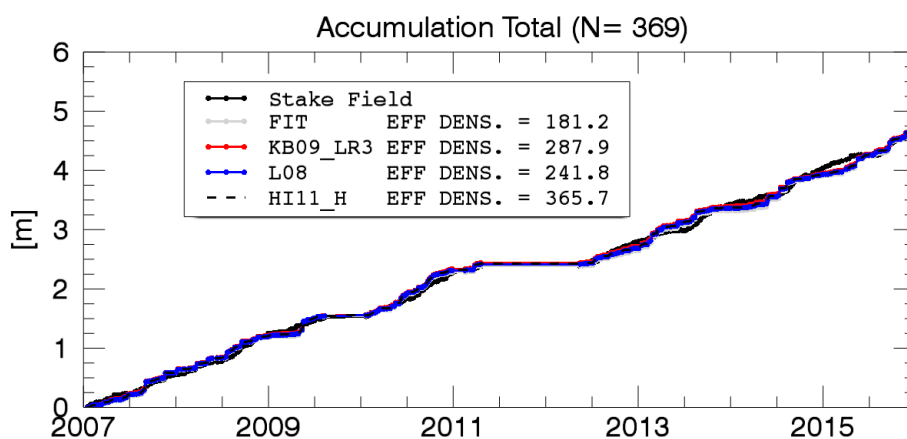


Figure 20: Total snowfall from CloudSat and stake field for all 369 weeks where data was available for both observation types.

Based on the findings presented in section 3.2.4, we will from here on apply the three Z-S relations that produce realistic effective densities and average them to obtain a final surface snowfall estimate for each CloudSat observation. The spread between the three relations will be used to determine an uncertainty range.

3.2.5 Final form of CloudSat snowfall retrieval over the GrIS

Based on the findings in the previous sections, the final CloudSat processing used from here on consists of three steps:

- (1) Correct for topography issues and identify the lowermost radar bin above the surface not affected by ground clutter using the IceBridge BedMachine topography as outlined in section 3.2.1. This step results in a set of radar reflectivities observed by CloudSat typically at altitudes around 1200 m above the surface.
- (2) Correct the so-obtained reflectivities for the height difference between their observation height (around 1200 m) and the surface following the method outlined in section 3.2.1 This step results in a set of height-corrected reflectivities.
- (3) Apply the three Z-S relations ('HI11_H', 'KB09_LR3', and 'L08', see section 3.2.4) to convert those reflectivities to equivalent snowfall rates. Average the three estimates to get a final surface snowfall estimate. Use the spread between the three as an uncertainty estimate.

In the entire process, we use the official CloudSat SNOWPROF product solely to determine the precipitation type. That is, only if the SNOWPROF product reports snowfall, we use the snowfall rate derived according to the approach outlined above. This screens out high reflectivity cases associated

with rainfall. The so-derived snowfall rates will form the basis of all further validation and discussion from here on.

3.2.6 Comparison against GC-NET and PROMICE

Similar to the results presented in section 3.2.4, we compare accumulation results for various GC-NET and PROMICE stations with CloudSat-derived snowfall rates. We limit the comparisons to monthly mean accumulation to allow for enough CloudSat observations to enter the comparison. GC-NET and PROMICE accumulation values are calculated based on sonic height measurements, which are reported daily (GC-NET) and hourly (PROMICE). For each of these hourly or daily accumulation periods, we find CloudSat observations within 50 km from the surface station. For each accumulation period where both CloudSat and surface observations are available and the temperature at the surface does not exceed freezing, we then calculate the average snowfall and accumulation rate. We limit the analysis to temperatures below freezing in order to avoid snowmelt affecting the sonic height estimates.

For each month, this procedure leads to a set of combined surface sonic and CloudSat derived accumulation and snowfall rates. Similar to the discussion on the stake field further up, the mean ratio of these two then defines the effective density needed to explain the accumulation with CloudSat snowfall.

Comparing CloudSat accumulation to PROMICE and GC-NET

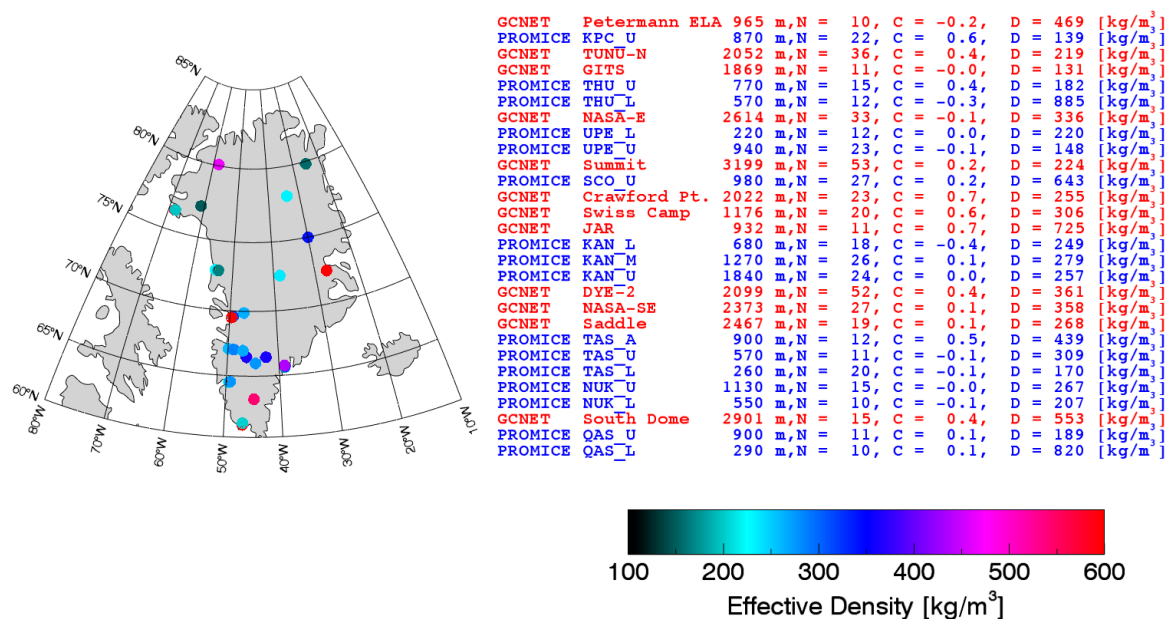


Figure 21: Effective density of snowfall to explain surface accumulation from GC-NET or PROMICE by CloudSat snowfall. The table shows station name as well as elevation, and N: Number of months with valid data, C: Correlation between surface accumulation and CloudSat, D: effective density. The effective density at each site is also indicated on the map by its colour.

Out of all PROMICE and GC-NET stations, a total of 28 produced enough data (see Figure 21). The derived effective density varies widely between 130 and 890 kg/m³. The large spread in densities is owed mostly to the relatively noisy sonic data as well as to imperfect temporal and spatial colocations between CloudSat and the surface observations. The average density is 343±205 kg/m³, or 287±127 kg/m³ if the outliers above 700 kg/m³ (e.g. station 'JAR') are removed from the dataset.

Recent results by *Fausto et al.* [2018] indicate an average density of the uppermost snow layer over Greenland to be 315±44 kg/m³ for the uppermost 10 cm and 341±37 kg/m³ for the uppermost 50 cm or roughly 5 - 15% higher than our findings.

Fausto et al. [2018] as well as earlier studies (e.g. *Reeh et al.* [2005]) also find a weak dependency of density on temperatures which seems also present in our results where density and mean station temperature are weakly correlated with correlation coefficients of C=0.24 and C=0.23 if the outliers above 700 kg/m³ (e.g. station 'JAR') are removed from the dataset. As can be seen from Figure 22, the dataset is very noisy.

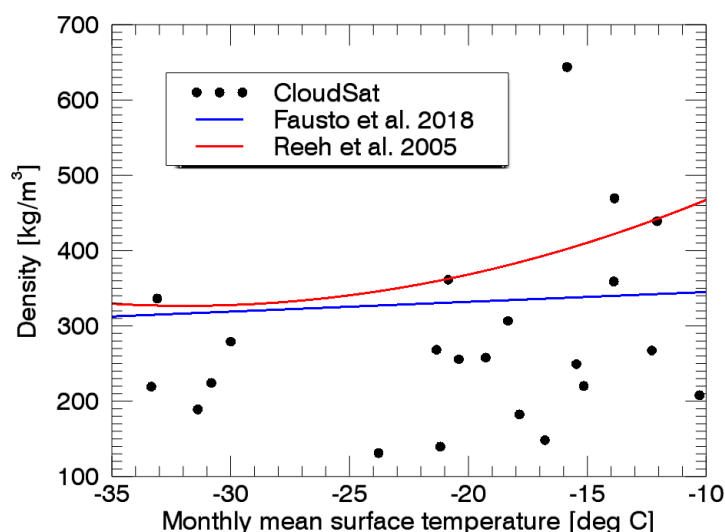


Figure 22: Density as function of mean station temperature for the 28 cases shown in Figure 21. The red and blue curves show results from *Fausto et al.* [2018] and *Reeh et al.* [2005].

In summary, the results of the comparison between CloudSat and GC-NET or PROMICE indicate some general broad agreement with earlier studies. However, the direct comparisons are hampered by colocation issues and noisy sonic data, so that no definite conclusions can be drawn from this comparison. The comparison to the stake field observations in section 3.2.4 provides less noisy and more conclusive evidence for the value of CloudSat data.

3.3 Spatial and seasonal variability of snowfall over the GrIS

Using the strategy laid out in Section 3.2.5, we derive monthly mean CloudSat estimates over the GrIS for all months where CloudSat data are available and at a resolution of 1×2 degrees, which roughly corresponds to 110×110 km² at 60° N. In comparison, the resolution of ERA-Interim at 60° N is 0.7×0.7

degrees or $78 \times 39 \text{ km}^2$. Figure 23 shows the annual mean values for CloudSat and ERA as well as their relative difference in percent. Figure 24 shows the annual cycle over the GrIS.

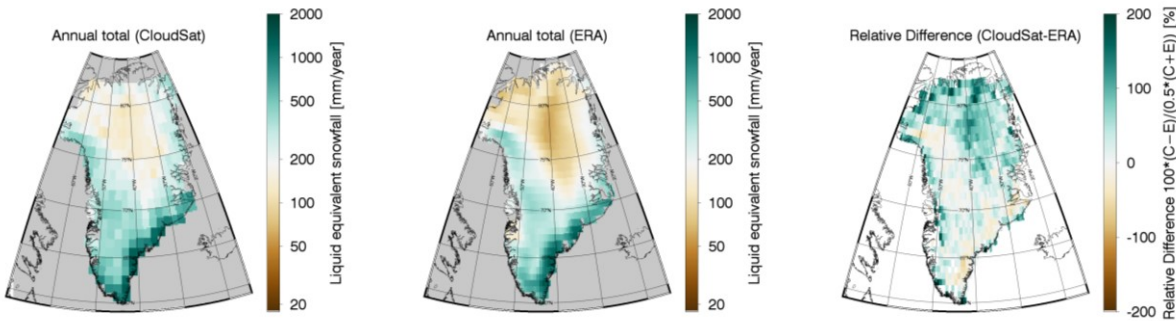


Figure 23: Annual mean liquid equivalent snowfall from CloudSat (left panel), ERA-Interim (2006-2016, middle panel), and the relative difference between both (right panel).

Marked differences between ERA-Interim and CloudSat exist in the months June-September, where ERA shows less precipitation over the GrIS than CloudSat. For the summer months, the spatial correlation between ERA and CloudSat is also worst. Differences are most pronounced over the high GrIS north of 72° N , where ERA shows very little precipitation. These differences can also be identified in the monthly snowfall plots shown in Figure 25 and Figure 26. It is interesting to note that the area where ERA-Interim seems to underestimate snowfall coincides nearly perfectly with areas where the CloudSat-derived snowfall is associated with low, cumuliform snowfall (see Figure 10a in *Kulie et al. (2016)*). The months with the highest positive bias (Figure 24 bottom left panel) also show the lowest spatial correlation between ERA-Interim and CloudSat snowfall estimates (Figure 24 top right panel).

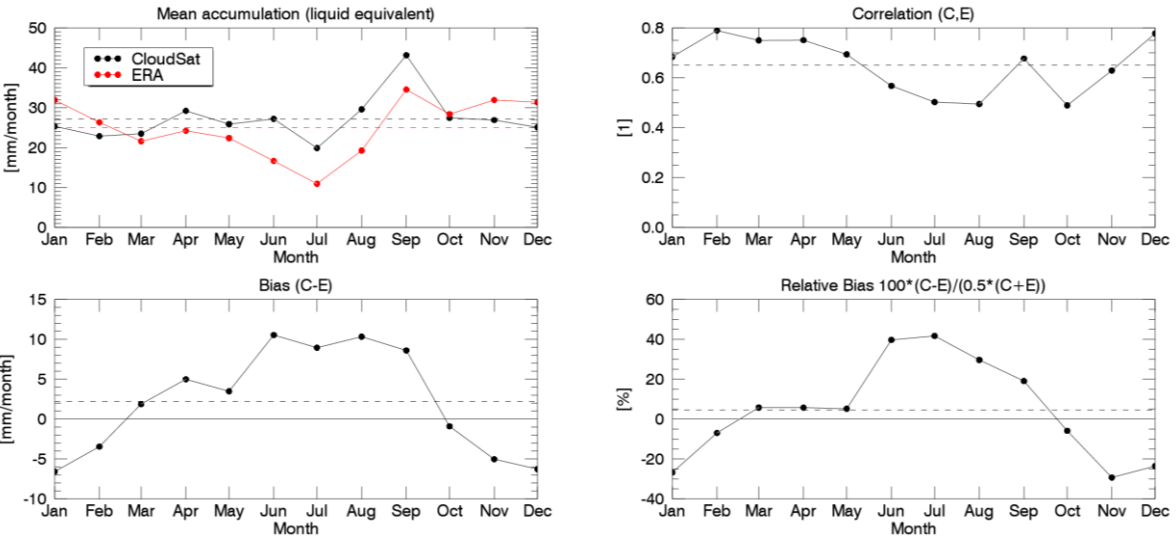


Figure 24: Annual cycle of liquid equivalent snowfall over the GrIS from CloudSat and ERA-Interim (top left panel), spatial correlation between the two (top right), mean bias (bottom left) and mean relative bias (bottom left). The dashed horizontal lines represent the annual average.

Total snowfall over the GrIS from CloudSat adds up to 34 ± 7.5 cm/yr liquid equivalent, where the uncertainty range is given by the spread in Z-S relations. The corresponding ERA-Interim derived estimate is 30 cm/yr. Comparing these results to earlier publications (see Table 1 in *Cullather et al.* [2014]), we find our ERA-Interim derived estimate to be lower. The snowfall various values reported in *Cullather et al.* [2014] show a wide spread depending on which model is used. Note further that the values in *Cullather et al.* [2014] refer to total precipitation, whereas our values represent snowfall only. *Ettema et al.* [2009] find a fraction of 6 % liquid and 94% snow over the GrIS, which can only partly explain the bias we see for ERA-Interim compared to *Cullather et al.* [2014]. Snowfall rates from CloudSat are in much better agreement with other studies. For example, *Ettema et al.* [2009] report snowfall over the GrIS based on high-resolution model simulations to be 40.7 cm/year (94% of their total precipitation), which is higher than both the CloudSat and ERA-Interim estimates reported here, but still in agreement with CloudSat within the range of uncertainty provided above.

Figure 25 and Figure 26 show the monthly mean spatial distribution of snowfall from CloudSat (Figure 25) and ERA-Interim (Figure 26), respectively. Both datasets identify a band along the southwest coast of Greenland, where snowfall in summer is near zero. These coastal areas are presumably too warm in summer for snow to reach the ground before melting. Note that the CloudSat data are at a coarser (1×2 degree) resolution than the ERA-Interim data, which explains this narrow coastal feature to be less pronounced in CloudSat compared to ERA.

=== REMAINDER OF PAGE DELIBERATELY LEFT EMPTY ===

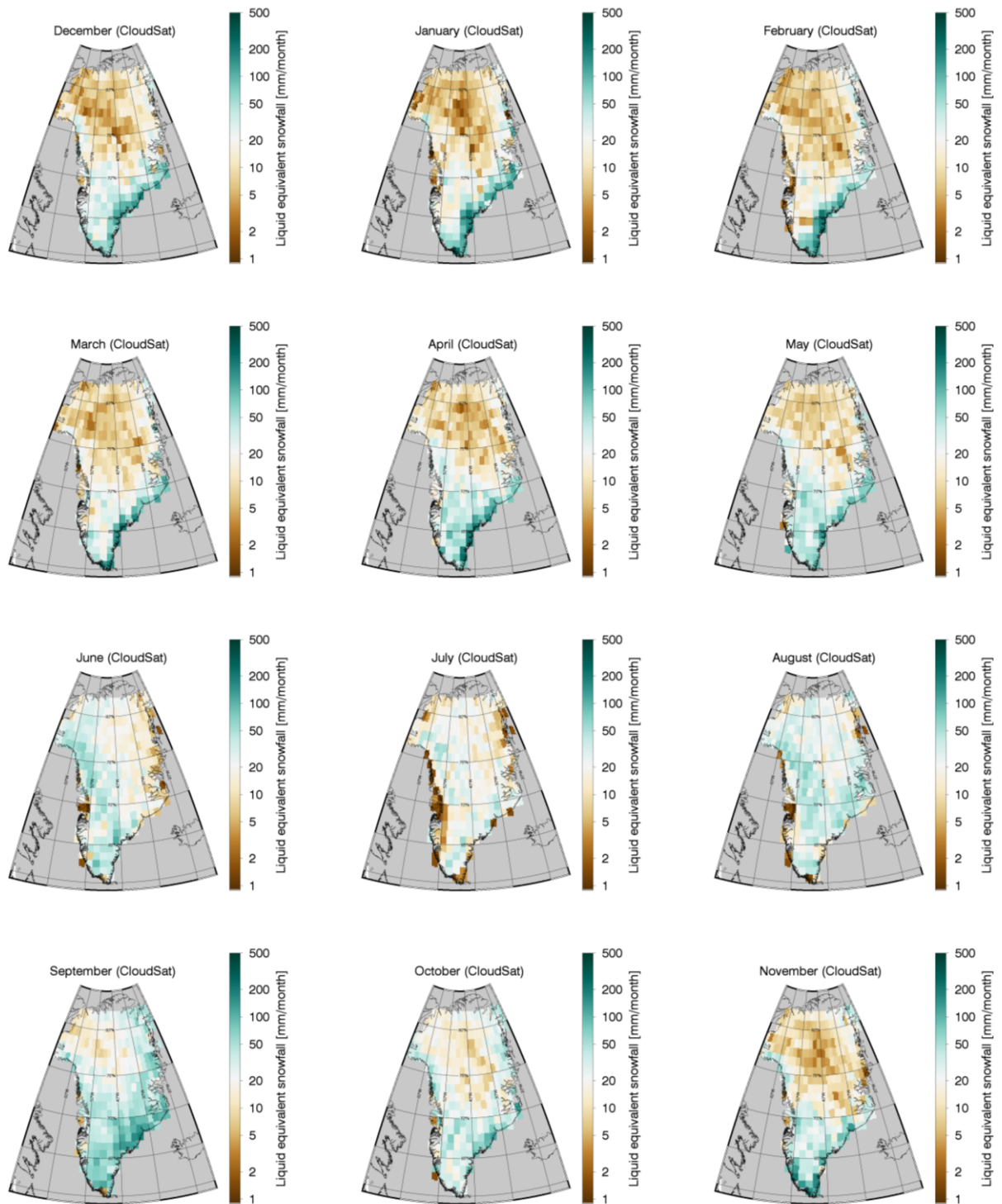


Figure 25: CloudSat-derived monthly mean snowfall rates.

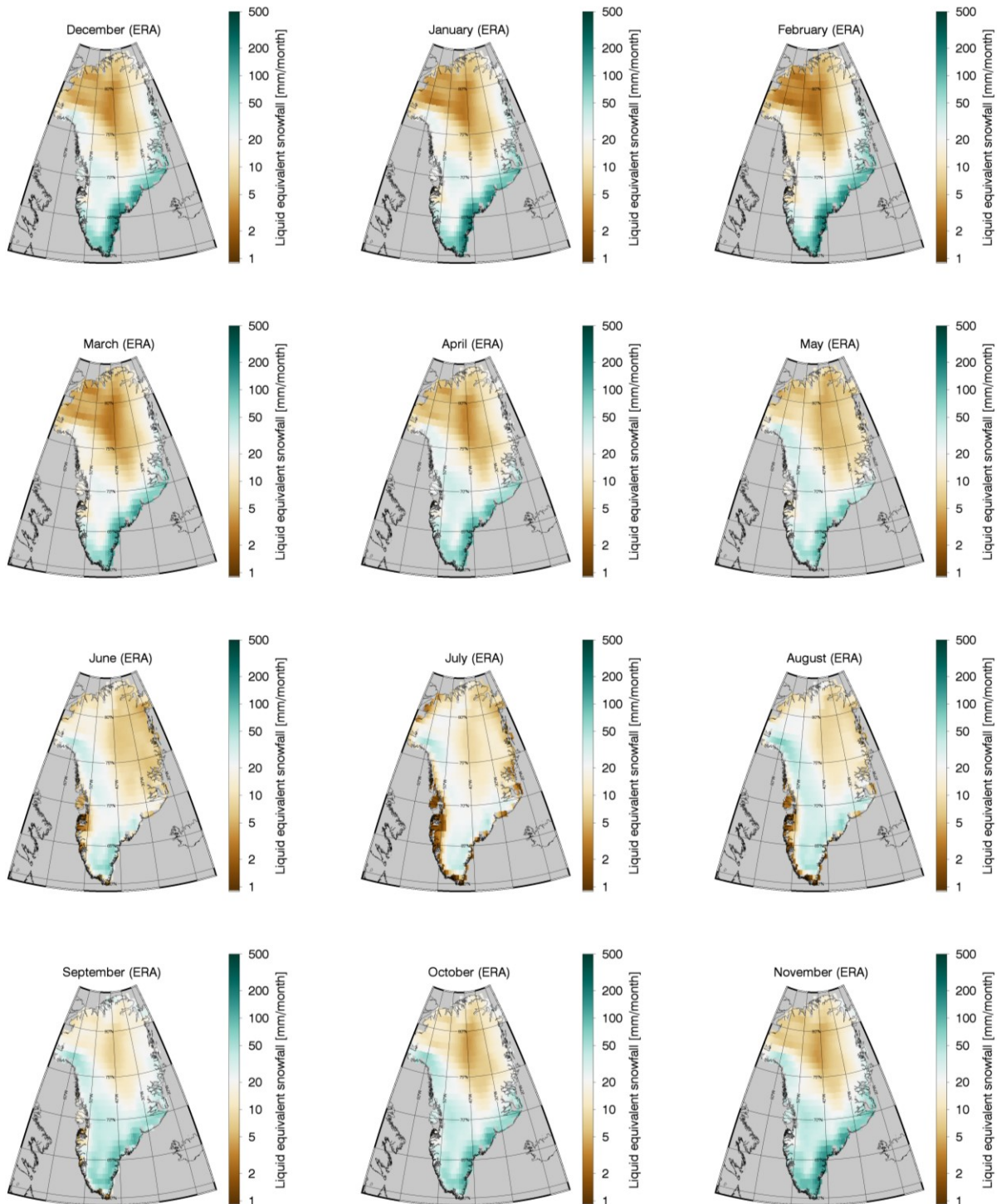


Figure 26: Same as Figure 25 but for ERA-Interim.

3.4 Snowfall by drainage system

As can be seen in Figure 23, even at resolution 1×2 degrees, the monthly CloudSat precipitation estimates over the GrIS are relatively noisy. As a nadir-looking instrument, CloudSat only provides few overpasses per grid-box per month. In addition to grid-box-averaged precipitation estimates, we therefore also evaluate CloudSat per major GrIS drainage system. We first binned CloudSat data onto the 0.7×0.7 degrees ERA-Interim grid and subsequently averaged these gridded data onto the drainage basins.

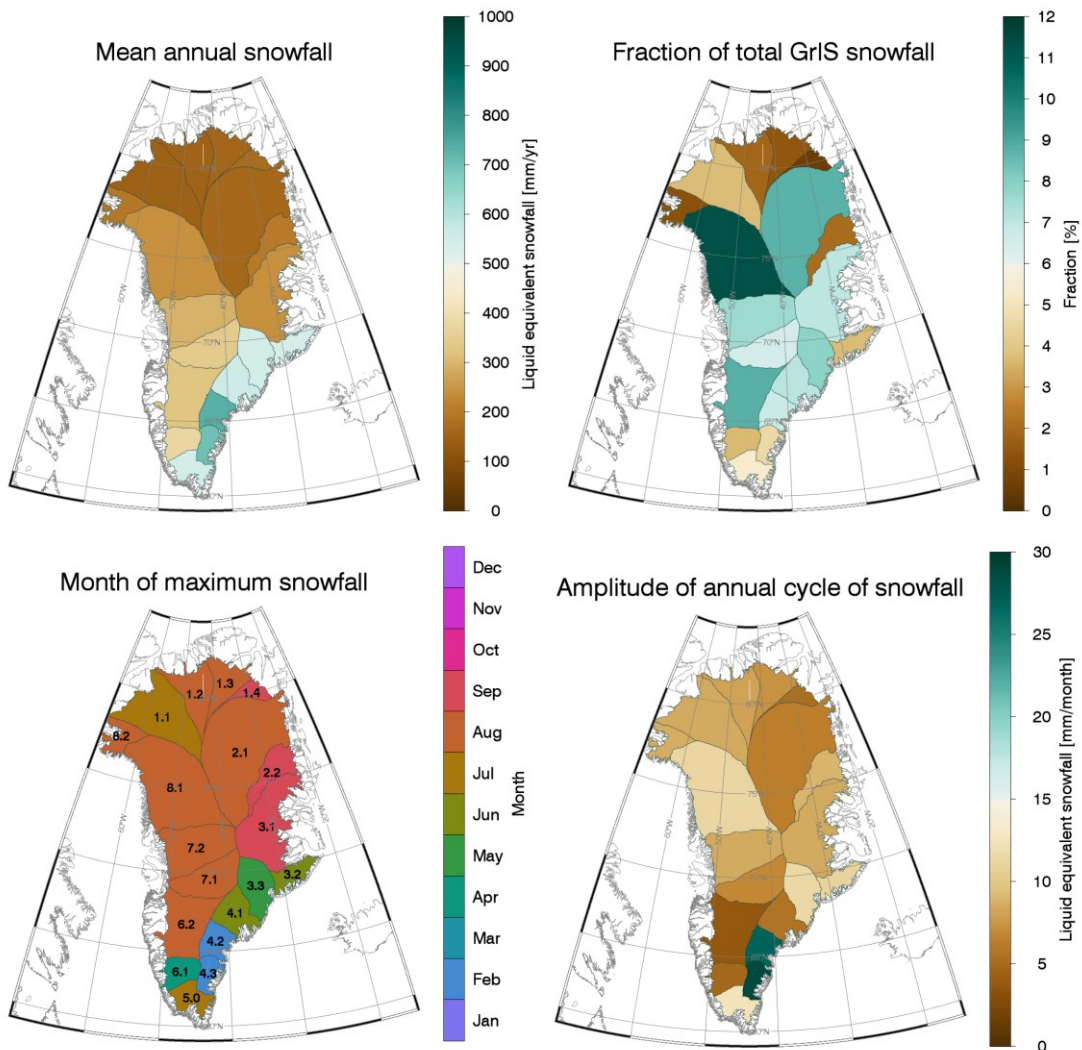


Figure 27: Annual snowfall associated with the different drainage systems defined by Zwally *et al.*, [2012]. The upper left plot shows the mean annual snowfall, the upper right plot shows the fractional contribution to the total snowfall over the GrIS, the lower left plot shows the month of maximum precipitation as well as the drainage-basin identifier used in Zwally *et al.* [2012], and the lower right plot shows the amplitude of the annual cycle of snowfall. The month of maximum precipitation and amplitude are derived using a cosine fit to the annual cycle (see Figure 28).

and ERA is strikingly good. The agreement in these areas seems to indicate that snowfall associated with cyclonic activity over the southeast of Greenland is represented well by ERA, whereas snowfall potentially associated with summertime precipitation is potentially under-represented in the model.

The dashed curves in Figure 28 are cosine fits of the annual cycle of precipitation, which are used to determine the months of maximum snowfall as well as the amplitude of snowfall reported in Figure 27. We note that these cosine fits do not necessarily correspond to physical features in the annual cycle of precipitation for all drainage systems, so that the values given for the annual cycle in Figure 27 should not be interpreted too strongly quantitatively. It does appear, however, that large parts of the central and north-western GrIS see maximum precipitation in summer, whereas the south-eastern part of the GrIS sees maximum precipitation in winter.

In the next section, we further investigate the differences between ERA-Interim and CloudSat based on monthly mean snowfall accumulation over Summit, where independent observational data are available.

3.5 Annual cycle of snowfall at Summit

Figure 29 compares monthly mean snowfall rates over Summit from all data sources discussed here. The stake field data have been corrected for sublimation/deposition using ERA estimates and converted to liquid equivalent snowfall in order to make results directly comparable to the other snowfall estimates.

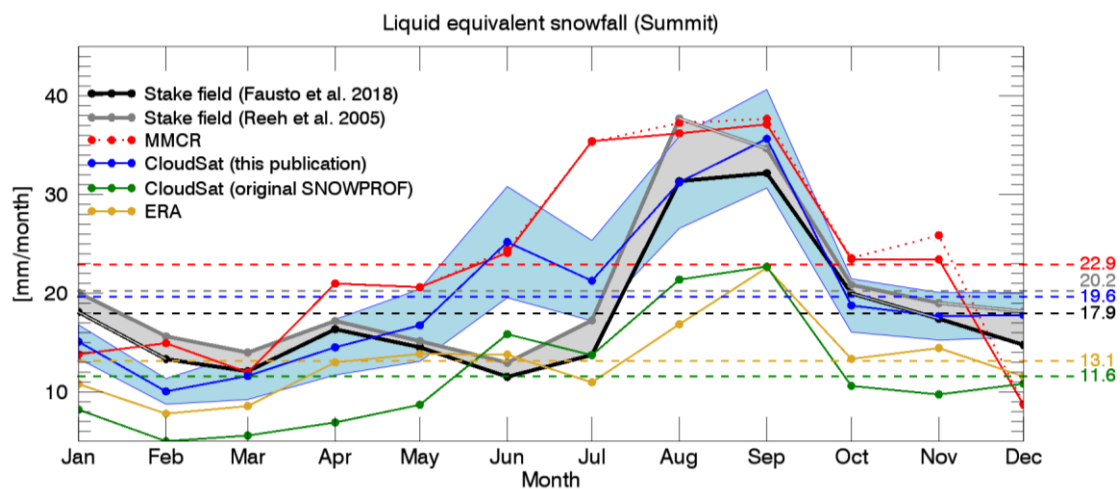


Figure 29: Liquid equivalent snowfall over Summit from different data sources used in this publication. The shaded uncertainty range around the CloudSat estimates gives the uncertainty due to Z-S relation. The shaded uncertainty range around the stake field estimates gives the uncertainty due to different assumptions about snow density. The stake field estimates presented herein have been corrected for sublimation/deposition using ERA-Interim sublimation/deposition estimates.

Cullen *et al.* [2014] study sublimation/deposition over the high GrIS in detail and find the contribution of sublimation/deposition to be generally around 2% of the total accumulation. On a monthly basis, values from ERA were a bit higher, but still did not significantly alter the stake field values. The CloudSat snowfall estimates agree well with the stake field observations with the exception of June

and July, where CloudSat (as well as MMCR) report much higher snowfall than the stake field. A similar discrepancy between June/July stake field observations and other snowfall measurements was already reported by *Dibb and Fahnestock* [2004]. *Castellani et al.* [2015], in their Figure 4, show a similar behaviour. Notably, June and July are the months with the highest inter-annual variability in snowfall. For completeness, we have also included the annual cycle based on the original CloudSat SNOWPROF retrieval (green). One can see that using the SNOWPROF surface snowfall rate retrieval without the corrections discussed and applied herein would yield a precipitation estimate lower than ERA and would also fail to show the strong annual cycle seen in the other observational datasets.

3.6 Relation between liquid equivalent snowfall rate and snow water equivalent (SWE)

In this section, we discuss the relevance of space-borne observations of falling snow (e.g. through CloudSat) for the validation of snow water equivalent (SWE) estimates that are routinely derived from passive microwave instruments, radar, or lidar altimeters. Representing the amount of all water stored in a snow layer, a simple budget equation for SWE can be set up at large-enough scales where horizontal redistribution of snowpack does not play a role:

$$\frac{dSWE}{dt} = SR + RR - SUBLIM - RUNOFF, \quad (3)$$

where the individual terms represent:

- SR: Liquid equivalent snowfall rate. This is directly accessible from CloudSat.
- RR: Rain rate on snowpack. This has to be considered as rainwater stored in or on the snowpack will still count toward SWE.
- SUBLIM: Sublimation/evaporation from the snowpack or deposition onto the snowpack.
- RUNOFF: Runoff of liquid water from the snowpack, created either by rain or by melting. Meltwater stored in or on the snowpack will still count toward SWE.

Space-based measurements of falling snow, such as the ones from CloudSat, directly provide SR which is the most important source term of SWE. The other terms, with the possible exception of RR, are not directly accessible from satellite observations. However, under restricted circumstances some of the above effects can be ignored. In particular over the GrIS, the following can be assumed:

- Sublimation/deposition from/to the snowpack is small compared to the snowfall rate. *Cullen et al.* [2014] study sublimation/deposition over the high GrIS in detail and find the contribution of sublimation/deposition to be generally around 2% of the total accumulation. These values are in general agreement with the deposition/sublimation values used in this study based on ERA-Interim. Therefore, the SUBLIM term in the above equation can be corrected for without significant loss in accuracy.

- Over large parts of the higher GrIS, the surface temperatures never exceed freezing for several months. During those months, all precipitation falls as snow so that the terms RR and RUNOFF are near zero.

Based on these considerations, a viable approach for SWE comparisons/validation would be:

- (1) Select areas and corresponding months (e.g. 1x2 degree geographical grids boxes) where the monthly maximum surface temperature does not exceed zero degrees Celsius (e.g. from ERA-Interim).
- (2) Calculate monthly mean liquid equivalent snowfall rates (i.e. SR in Eq (3)) from CloudSat for those areas and months.
- (3) Estimate sublimation/deposition from model data, e.g. ERA-Interim. If this term is sufficiently small compared to the SR, it can be used to correct the SR.
- (4) Comparisons between CloudSat-derived SR and other SWE products would then be possible on a monthly basis and for selected areas.

Figure 30 shows the average number of months per year where the maximum surface temperature never exceeds freezing based on ERA-Interim diurnal maximum temperatures. Large parts of the high GrIS never exceed freezing, but also areas in the wider Arctic as far south as 60° N do not exceed freezing for one to several months a year. Comparing monthly SR from CloudSat with SWE products for this entire region would yield a sizeable comparison dataset.

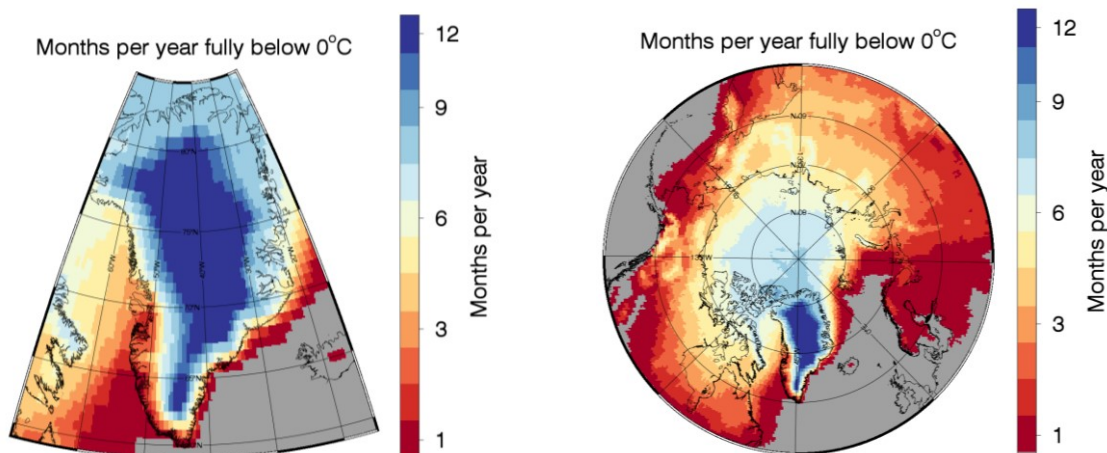


Figure 30: Average number of months per year in which the maximum surface temperature never exceeded zero degrees Celsius in the period 2006-2016 based on ERA-Interim diurnal maximum temperatures.

4 Science potential of observations in support of future missions

The existing observing system over the GrIS provides ample opportunity for support of a diverse set of future missions. Long-term observations of standard surface variables (temperature, pressure, wind) as well as of spectrally integrated surface radiative fluxes are available for a variety of different sites from GC-NET and PROMICE. This report details the use of ground-based observational for validation of space-based snow accumulation over the GrIS in particular.

Snow accumulation is not measured directly by the GC-NET and PROMICE automatic weather stations (AWS) but inferred from surface height changes measured by sonic ranging devices mounted on the mast of the AWS. Our evaluation of these data provides reasonable comparisons between space-based CloudSat observations and snow accumulation at these surface stations. However, the sonic-based accumulation estimates are relatively noisy and comparisons with other ground-based observations at Summit also show potential systematic issues with some of the accumulation estimates.

The Summit observatory plays a critical role in evaluating space-based observations of precipitation over the GrIS. It provides independent observations of weekly snowfall accumulation via a bamboo stake field. These data go back to 2007. Furthermore, the ICECAPS experiment provides upward-looking radar observations of precipitation going back to 2010 with a likely end date of summer 2020. The validation results in this report rely heavily on this unique dataset.

Based on the findings in this report, the following recommendations in support of future precipitation missions can be drawn:

- a) In order to validate space-based snowfall estimates over the GrIS, at least one reference station over the higher GrIS should be maintained and provide routine observations of precipitation with an upward-looking radar, accompanied by regular ground-based accumulation observations at not too long temporal intervals (ideally weekly). Currently, Summit Station is well equipped to fill this role. It is unclear if after summer 2020 radar observations will remain available at Summit.
- b) Given the validation results reported here, we are confident that space-based radar observations from CloudSat and, in the future, EarthCare, will allow mapping of surface precipitation over the GrIS at an accuracy high enough to validate large-scale accumulation at seasonal temporal scales and spatial scales of the size of individual drainage basins. The nadir-only observation geometry of CloudSat and EarthCare hampers evaluation at spatial scales finer than $100 \times 100 \text{ km}^2$.
- c) Future space-based precipitation missions with scanning radars might provide even more information about snowfall over the GrIS. However, minimum detection thresholds need to be low enough for such instruments, as 50 % of the precipitation falling over the high GrIS is associated with reflectivities between -15 dBz and $+5 \text{ dBz}$. Another important factor is the range resolution of future radars that needs to be carefully tuned so as to avoid ground clutter issues in particular when shallow precipitation is dominant.
- d) With the caveats mentioned under b) and c), space-based radars can also help provide validation datasets for other missions, such as radar or lidar altimeter missions. If integrated

over large enough temporal and spatial scales, the radar-derived precipitation accumulation adjusted for sublimation/deposition should equal surface height change observed by altimeter to within the accuracy of the snowpack density needed to convert from liquid equivalent precipitation to geometric surface height change from accumulation.

- e) Comparison to SWE derived from other sensors will be possible for a relatively large subset of the data. Direct comparisons on e.g. a monthly mean basis would be possible in regions where for a given month the temperatures do not exceed zero degrees Celsius. In Section 3.6 we have laid out a detailed plan how such comparisons could be performed.

Based on these considerations, our top-level recommendation is to maintain at least one long-term surface station over the high GrIS that provides precipitation observations from upward-looking radar as well as from other ground-based precipitation measurement devices. Such a station can help validate and anchor space-based observation of snowfall as well as accumulation observations from altimeters. With the anticipated end of ICECAPS in summer 2020, such observations would be missing.

5 References

- Belleflamme, A., X. Fettweis, and M. Ericum (2015), Recent summer Arctic atmospheric circulation anomalies in a historical perspective, *The Cryosphere*, 9(1), 53-64, doi:10.5194/tc-9-53-2015.
- Berdahl, M., A. Rennermalm, A. Hammann, J. Mioduszewski, S. Hameed, M. Tedesco, J. Stroeve, T. Mote, T. Koyama, and J. R. McConnell (2018), Southeast Greenland Winter Precipitation Strongly Linked to the Icelandic Low Position, *J Climate*, 31(11), 4483-4500. doi:10.1175/jcli-d-17-0622.1.
- Box, J., and K. Steffen (2000), Greenland Climate Network (GC-NET) Data Reference Rep.
- Castellani, B. B., M. D. Shupe, D. R. Hudak, and B. E. Sheppard (2015), The annual cycle of snowfall at Summit, Greenland, *J Geophys Res-Atmos*, 120(13), 6654-6668, doi:10.1002/2015jd023072.
- Cullather, R. I., S. M. J. Nowicki, B. Zhao, and M. J. Suarez (2014), Evaluation of the Surface Representation of the Greenland Ice Sheet in a General Circulation Model, *J Climate*, 27(13), 4835-4856. doi:10.1175/jcli-d-13-00635.1.
- Cullen, N. J., T. Mölg, J. Conway, and K. Steffen (2014), Assessing the role of sublimation in the dry snow zone of the Greenland ice sheet in a warming world, *Journal of Geophysical Research: Atmospheres*, 119(11), 6563-6577. doi:10.1002/2014jd021557.
- Dibb, J. E., and M. Fahnestock (2004), Snow accumulation, surface height change, and firn densification at Summit, Greenland: Insights from 2 years of in situ observation, *Journal of Geophysical Research*, 109(D24). doi:10.1029/2003jd004300.
- Ettema, J., M. R. van den Broeke, E. van Meijgaard, W. J. van de Berg, J. L. Bamber, J. E. Box, and R. C. Bales (2009), Higher surface mass balance of the Greenland ice sheet revealed by high-resolution climate modeling, *Geophys Res Lett*, 36(12). doi:10.1029/2009gl038110.
- Fausto, R. S., et al. (2018), A Snow Density Dataset for Improving Surface Boundary Conditions in Greenland Ice Sheet Firn Modeling, *Frontiers in Earth Science*, 6. doi:10.3389/feart.2018.00051.
- Hanna, E., T. E. Cropper, P. D. Jones, A. A. Scaife, and R. Allan (2015), Recent seasonal asymmetric changes in the NAO (a marked summer decline and increased winter variability) and associated changes in the AO and Greenland Blocking Index, *International Journal of Climatology*, 35(9), 2540-2554, doi:10.1002/joc.4157.
- Hiley, M. J., M. S. Kulie, and R. Bennartz (2011), Uncertainty Analysis for CloudSat Snowfall Retrievals, *J Appl Meteorol Clim*, 50(2), 399-418, doi:10.1175/2010jamc2505.1.
- Hong, G. (2007), Parameterization of scattering and absorption properties of nonspherical ice crystals at microwave frequencies, *Journal of Geophysical Research-Atmospheres*, 112(D11), -.
- Kulie, M. S., and R. Bennartz (2009), Utilizing Spaceborne Radars to Retrieve Dry Snowfall, *J Appl Meteorol Clim*, 48(12), 2564-2580, doi:10.1175/2009jamc2193.1.
- Kulie, M. S., R. Bennartz, T. J. Greenwald, Y. Chen, and F. Weng (2010), Uncertainties in Microwave Properties of Frozen Precipitation: Implications for Remote Sensing and Data Assimilation, *Journal of the Atmospheric Sciences*, 67(11), 3471-3487, doi:10.1175/2010jas3520.1.
- Liu, G. S. (2008), A Database of Microwave Single-Scattering Properties for Nonspherical Ice Particles, *Bulletin of the American Meteorological Society*, 89(10), 1563-+.
- Matrosov, S. Y. (2007), Modeling backscatter properties of snowfall at millimeter wavelengths, *Journal of the Atmospheric Sciences*, 64(5), 1727-1736.

Morlighem, M., et al. (2017), BedMachine v3: Complete Bed Topography and Ocean Bathymetry Mapping of Greenland From Multibeam Echo Sounding Combined With Mass Conservation, *Geophys Res Lett*, 44(21), 11051-11061. doi:10.1029/2017GL074954.

Pettersen, C., R. Bennartz, A. J. Merrelli, M. D. Shupe, D. D. Turner, and V. P. Walden (2017), Precipitation regimes over central Greenland inferred from 5 years of ICECAPS observations, *Atmospheric Chemistry and Physics Discussions*, 1-48, doi:10.5194/acp-2017-857.

Reeh, N., D. A. Fisher, R. M. Koerner, and H. B. Clausen (2005), An empirical firn-densification model comprising ice lenses, *Annals of Glaciology*, 42, 101-106

Seo, K. W., D. E. Waliser, C. K. Lee, B. J. Tian, T. Scambos, B. M. Kim, J. H. van Angelen, and M. R. van den Broeke (2015), Accelerated mass loss from Greenland ice sheet: Links to atmospheric circulation in the North Atlantic, *Global and Planetary Change*, 128, 61-71, doi:10.1016/j.gloplacha.2015.02.006.

Sheppard, B. E., and P. I. Joe (2008), Performance of the Precipitation Occurrence Sensor System as a Precipitation Gauge, *Journal of Atmospheric and Oceanic Technology*, 25(2), 196-212, doi:10.1175/2007jtecha957.1.

Shupe, M. D., et al. (2013), High and Dry: new Observations of Tropospheric and Cloud Properties above the Greenland ice Sheet, *B Am Meteorol Soc*, 169-186.

Stephens, G. L., et al. (2002), The CloudSat mission and the a-train - A new dimension of space-based observations of clouds and precipitation, *Bulletin of the American Meteorological Society*, 83(12), 1771-1790.

Stephens, G. L., et al. (2008), CloudSat mission: Performance and early science after the first year of operation, *Journal of Geophysical Research-Atmospheres*, 113(D23), doi:10.1029/2008jd009982.

Tanelli, S., S. L. Durden, E. Im, K. S. Pak, D. G. Reinke, P. Partain, J. M. Haynes, and R. T. Marchand (2008), CloudSat's Cloud Profiling Radar After Two Years in Orbit: Performance, Calibration, and Processing, *IEEE Transactions on Geoscience and Remote Sensing*, 46(11), 3560-3573.

van As, D. (2017), The Programme for Monitoring of the Greenland Ice Sheet: PROMICE science report 2016Rep., 73 pp, Geological Survey of Denmark and Greenland (GEUS)

van den Broeke, M., J. Bamber, J. Ettema, E. Rignot, E. Schrama, W. J. van de Berg, E. van Meijgaard, I. Velicogna, and B. Wouters (2009), Partitioning recent Greenland mass loss, *Science*, 326(5955), 984-986, doi:10.1126/science.1178176.

Wood, N. B., T. S. L'Ecuyer, A. J. Heymsfield, G. L. Stephens, D. R. Hudak, and P. Rodriguez (2014), Estimating snow microphysical properties using collocated multisensor observations, *J Geophys Res-Atmos*, 119(14), 8941-8961, doi:10.1002/2013jd021303.

Zwally, H. J., M. B. Giovinetto, M. A. Beckley, and J. L. Saba (2012), Antarctic and Greenland Drainage Systems, GSFC Cryospheric Sciences Laboratory, http://icesat4.gsfc.nasa.gov/cryo_data/ant_grn_drainage_systems.php.

Appendix A: GC-NET and PROMICE datasets and data formats

Hourly GC-NET and PROMICE observations are provided in a single NetCDF file (`surface_stations.nc`). This file holds the data listed in Table 3:

Table 3: Variables contained in `surface_stations.nc`.

Variable name	Description	Variable type	Units	Missing value	Comments
LAT	Station latitude	Float	Degrees North	N/A	
LON	Station longitude	Float	Degrees East	N/A	
ELEV	Station elevation	Float	Meters above Mean Sea Level	N/A	
NAME	Station name	String array of length 46	Name of station in network	N/A	Station names for 46 surface stations
NETWORK	Network name	String array of length 46	'PROMICE' or 'GCNET'	N/A	
TIME	Time	Float array of length 184080	Days since 1950-01-01 00:00:00.0"	-999	184080 hourly values from 1995-01-01 until 2015-12-31
TEMP	Temperature 2-3 m above surface	Float array of length 46 × 184080	Kelvin	-999	
RH	Relative humidity 2-3 m above surface	Float array of length 46 × 184080	Percent	-999	Relative humidity defined over ice
WIND	Wind speed near surface 2-3 m above surface	Float array of length 46 × 184080	m/s	-999	
SONIC_HEIGHT	Height of sonic above surface	Float array of length 46 × 184080	m	-999	
TSFC_IR	Surface temperature from IR	Float array of length 46 × 184080	K	-999	

Appendix B: ICECAPS datasets and data formats

ICECAPS observations are provided in a single NetCDF file (`icecaps_data.nc`) every minute. This file holds the data listed in Table 4.

Table 4: Variables contained in `icecaps_data.nc`

Variable name	Variable description	Variable type	Units	Missing value	Comments
TIME	Time	Float array of length 2868480	Days since 1950-01-01 00:00:00.0"	-999	2848680 values, every minute from 2010-07-13 until 2015-12-25
TEMP2M	Temperature 2m above surface	Float array of length 2868480	Kelvin	-999	
TEMP10M	Temperature 10m above surface	Float array of length 2868480	Kelvin	-999	
RH	Relative humidity 2m above surface	Float array of length 2868480	percent	-999	Relative humidity defined over ice
WINDSPEED	Wind speed 10 m above surface	Float array of length 2868480	m/s	-999	
WINDDIR	Wind direction 10 m above surface	Float array of length 2868480	degrees	-999	
PRESSURE	Surface pressure	Float array of length 2868480	hPa	-999	
SNOW_CLASS	Snowfall type classification	Byte array of length 2868480	0 = IC 1 = CLW 2 = indetermin.	-999	Classification following <i>Pettersen et al.</i> [2017]
POSS_SR	Snowfall rate from POSS	Float array of length 2868480	mm/hr	-999	Snowfall rate following <i>Pettersen et al.</i> [2017]
ALT	Radar beam altitude	Float array of length 134	m	-999	
REFL	MMCR Radar reflectivity	Float array of length 134 × 2868480	dBz	-999	

Appendix C: CloudSat monthly mean liquid equivalent snowfall rates

CloudSat-average monthly mean snowfall rates (see Figure 23) and uncertainties are provided in a single NetCDF file (**cloudsat_1x2_degree.nc**) at 1x2 degree resolution. This file holds the data listed in Table 5.

Table 5: Variables contained in cloudsat_1x2_degree.nc

Variable name	Variable description	Variable type	Units	Missing value	Comments
TIME	Time	Float array of length 12	Months	-999	
LATITUDE	Center latitude of 1x2 degree grid box	Float array of length 26	Degrees North	-999	
LONGITUDE	Center longitude of 1x2 degree grid box	Float array of length 33	Degrees East	-999	
SR	Monthly mean liquid equivalent snowfall rate	Float array of length 12 x 33 x 26	mm/month liquid equivalent	-999	
DSR	Uncertainty of monthly mean liquid equivalent snowfall rate	Float array of length 12 x 33 x 26	mm/month liquid equivalent	-999	Uncertainty caused by Z-S relation. See section 3.2.5

Additionally, monthly mean snowfall rates and uncertainties are also provided per catchment area in a single NetCDF file (**cloudsat_catchment.nc**). This file holds the data listed in Table 6.

Table 6: Variables contained in cloudsat_catchment.nc

Variable name	Variable description	Variable type	Units	Missing value	Comments
TIME	Time	Float array of length 12	Months	-999	
AREA_ID	ID number of catchment area	Float array of length 26	N/A	N/A	Area IDs following Zwally <i>et al.</i> [2012]
SR	Monthly mean liquid equivalent snowfall rate	Float array of length 12 x 33 x 26	mm/month liquid equivalent	-999	
DSR	Uncertainty of monthly mean liquid equivalent snowfall rate	Float array of length 12 x 33 x 26	mm/month liquid equivalent	-999	Uncertainty caused by Z-S relation. See section 3.2.5